Abstract

Contents

List of Figures

List of Tables

1 Introduction

(Note: Strong points for EAP use)

Dielectric elastomers (DEs) are polymers that are non conductive but polarize and deform under electrostatic excitation. These light weight, flexible and available polymers has the potential of being used and are emarging as actuators in a wide variety of applications such as artificial muscles, energy-harvesting devices, micropumps, and soft robotics, among many others [Carpi et al., 2011].

(Note: The microstructure and macrostructure of the EAP (polymer networks from chains and chains from monomers -> a polymer strip sandwiched between two electrodes)**)**

At the microscopic level, DEs have the hierarchical structure of networks of polymer chains. A polymer chain is a long string of repeating dipolar monomers. At the macroscopic level, the essential part of a DE based device is a thin soft membrane of the DE sandwiched between two compliant electrodes. When electric potential is applied between the electrodes the monomers react to the electric exitations while the DE membrane reduces its thickness as a result of the attraction between the two oppositely charged electrodes. Simultaneously, the membrane area expands due to Poisson's effect. This process converts electrical energy into mechanical energy. Attractive features of dielectric elastomers include large strain, fast response, silent operation, low cost and high efficiency [Moscardo et al., 2008].

(Note: The ratio between elastic moduli and dielectric moduli and its importance)

The electromechanical coupling in DEs is characterized by a quadratic dependence of the force between the electrodes on the applied electric potential [Toupin, 1956]. In turn, the deformation depends on the force via the elastic moduli. Thus, the coupling depends on the ratio between the dielectric and the elastic moduli. Commonly, flexible polymers have low dielectric moduli while high dielectric moduli polymers are usually stiff. Accordingly, since this ratio is relatively small, large electric potentials are needed for a meaningful actuation.

(Note: electric breakdown and other failure mechanisms)

The requirement for high electric potentials implies that the feasibility of these materials is limited by their dielectric strength, which is the limit beyond which electric current flows through the dielectric material [Pelrine et al., 2000]. This failure mechanism is known as electric breakdown or dielectric breakdown. In some cases this results in a transformation of the insulator into an electric conductor. In general, electrical breakdown may be a singular, a cyclic or a continuous event [Ahmad, 2012]. Predicting accurately the occurrence of an electrical breakdown, timing or position, is not yet possible mostly because it does not depend on a single cause, but it is a statistical product of several factors. The most notable factors are the local defects, such as a void or an inclusion that

would create a local decrease in the thickness of the DE, leading to higher electric fields or higher mechanical stresses [Vogan, 2004]. In practice the dielectric strength is measured experimentally [Vogan, 2004, Qiang et al., 2012] and is measured for a membrane at a given thickness with a given testing equipment [Madsen et al., 2016]. In their work Plante and Dubowsky [2006, 2007] examined the failure mechanisms and the performance boundaries of DEs. Their analysis showed that the performance of DEs made with highly viscoelastic polymer mambranes is governed by four key mechanisms which are electric breakdown, current leakage, pull-in failure and viscoelasticity.

(Note: The ratio between elastic moduli and dielectric moduli - low but can be improved**)**

A possible way to overcome the electric breakdown failure mechanism is by reducing the electric potentials that are currently needed for a meaningful actuation, this can be done by improving the polarizability of the DE. Several previous works suggest that the low ratio between the dielectric and the elastic moduli may be improved and thus their electromechanical response may be enhanced. A common general approach for improving this ratio involves inserting additional materials to the elastomer. This approach can result in a homogeneous or a composite elastomer. One aspect of the approach refers to embedding components with a higher dielectric constant, which can be classified as insulating or conducting, in a soft polymer [Huang et al., 2004, Stoyanov et al., 2010, Kofod et al., 2011]. Kussmaul et al. [2011] presented such a method for the electromechanical response enhancement of silicone elastomer networks, based on the grafting of molecules with high permanent dipoles to the crosslinker molecules. Their method also allows for a direct control of the mechanical properties of the elastomer by adjustments of the crosslinking density. Another aspect of the approach refers to improving the actuation in DEs with an appropriate adjustment of their microstructure as periodic laminates [deBotton et al., 2007, Tian et al., 2012, Rudykh et al., 2013, Lopez-Pamies, 2014, Volpini et al., 2019].

(Note: improving the response without changing the ratio between elastic moduli and dielectric moduli**)**

As a contrary to improving the ratio between the dielectric and elastic moduli, several works have been done to improve the responsiveness of DEs by adjusting the macroscopic structure of the actuators. These works are mainly in regards to soft robotics, but not limited to it [Jung et al., 2007, Rus and Tolley, 2015, Gu et al., 2017, Xu et al., 2017]. Recent works, such as Kellaris et al. [2018] and Rothemund et al. [2019] discussed soft electrohydraulic transducers, termed Peano-HASEL (hydraulically amplified self-healing electrostatic) actuators. Such actuators combine the strengths of fluidic actuators and electrostatic actuators. This combination is performed as the actuators are comprised of pouches, which are made of flexible dielectric polymer films, filled with a liquid dielectric and covered with compliant electrodes. When a voltage is applied to the electrodes, they

"zip" together due to the Maxwell stress, which causes the liquid inside the pouch to be displaced, and thus causes the contraction of the actuator [Rothemund et al., 2019].

(Note: Previous investigations of the polymer properties:)

(Note: Mechanical response)

The aspiration to affect the ratio between the dielectric and elastic moduli of DEs motivates a multiscale inquiry of their mechanical, dielectric and coupled properties. The response of polymers to purely mechanical loading across all scales was investigated extensively. A detailed investigation of the macroscopic behavior of soft materials undergoing large deformation is presented in Ogden [1997]. A pioneering analysis at the microscopic level was performed through the use of statistical mechanics by Kuhn and Grün [1942], which resulted in a Langevin based constitutive relation. This work led to a variety of multiscale models such as the three-chain model [Wang and Guth, 1952] and the eight-chain model [Arruda and Boyce, 1993]. Such an analysis of mechanical systems was also presented by Flory and Rehner [1943], Wall and Flory [1951] and James and Guth [1953] for rubberlike elasticity of polymer networks. A review of the development of statistical mechanics treatments of rubber elasticity was given in Treloar [1975]. Warner and Terentjev [2003] and Su and Purohit [2012] presented an analysis of mechanical systems through the use of statistical mechanics for liquid crystal elastomers.

(Note: Electrostatic response)

The response of polymers to electrostatic exitation was examined extensively at the macroscopic and microscopic scales by Tiersten [1990] and Hutter et al. [2007] among others. Discussing and analyzing constitutive relations for the macroscopic electric parameters, such as the polarization and the displacement, and for the microscopic electric parameters, such as the dipoles and the bound and free charge densities. Eringen [1963] presented an electrostatic theory for rigid bodies as theoretical ideal constructs while executing his analysis from a charge to a continuum.

(Note: Coupled response)

The analysis of the coupled electromechanical response of DEs at the macroscopic level began with the work of Toupin [1956]. Years later, Dorfmann and Ogden [2005] introduced the constitutive behavior of electro-sensitive elastomers via an invariant-based representation. This was expanded to the class of anisotropic materials by Bustamante [2008]. Among others, Zhao and Suo [2008] and Jimenez and McMeeking [2013] investigated the influence of the deformation and the rate of deformation on the electromechanical coupling. Lu et al. [2012] performed an analysis at the macroscopic level for the electromechanical response of membranes under a uniaxial force, under equal-biaxial forces and for the case of a membrane constrained in one direction and subject to a force in the other direction. Additionaly, they examined the response of a fiber-constrained membrane. A principle of virtual work for problems of combined electrostatic and mechanical

loading, which includes the interactions between the resulting strain and polarization, was presented by McMeeking et al. [2007]. Physically motivated multiscale analyses of the electromechanical coupling were previously performed by Cohen and deBotton [2014], Cohen and deBotton [2015] and Cohen and deBotton [2016]. Multiscale analysis that was based on statistical mechanics was introduced by Cohen et al. [2016].

(Note: Experimental work)

In addition to the discussed theoretical works, over the past 20 years the dielectric properties of DEs have been extensively investigated experimentally. Although some have determined the variation in the relative permittivity of DEs, such as VHB 4910/4905, under biaxial extension to be negligible, as can be seen in the works of Kofod et al. [2003] and Di Lillo et al. [2012] among others, several works contradicted those conclusions. Several investigations on the variation of the relative permittivity as a result of area stretch have revealed a decrease in its value. Choi et al. [2005] measured an initial relative permittivity $\epsilon_r = 4.4$ and $\epsilon_r = 2.25$ under area stretch of 9. Wissler and Mazza [2007] measured $\epsilon_r = 4.68$ and $\epsilon_r = 2.62$ as the initial relative permittivity and under area stretch of 25, respectively. Qiang et al. [2012] measured a decrease as well while performing a planar stretch of 16, as $\epsilon_r = 4.36$ was the initial permittivity and $\epsilon_r = 2.44$ was the measurement under stretch. Zhang et al. [1997] found from their experimental work on the electromechanical response of the polyurethane elastomer that the motions of chains can be divided to those related to the mechanical response and those related to the polarization response, while the overlap between them yields the electromechanical response. Some experimental works, such as Pelrine et al. [2000], Barnes et al. [2007] and Lu et al. [2012], examined the influence of prestraining the DEs membranes on the performance of actuators. These examinations were performed for biaxially and uniaxially prestraining silicone and acrylic elastomers. Furthermore, some work have been done into developing models that assist in estimating the variation in relative permittivity as a result of different stretch combinations [Jimenez and McMeeking, 2013, Dorfmann and Ogden, 2017]. An example of such work is the one presented in Cohen et al. [2017], where a statistical mechanics based model is compared to experimental findings.

(Note: This work)

(Note: A brief description of the displayed content)

We begin this work with a theoretical background, within the framework of continuum approach, concerning the mechanical, electrostatic and coupled cases. Following are a review of the analysis of the microstructure of isotropic polymer chain network using statistical mechanics through entrophy considerations and a reference of a phenomenological model for the electromechanical coupling of DEs that will be compared to our results. In section 3 an analysis of the DEs electroelasticity in several hierarchical cases, from a single electric charge to a network, is presented. Moreover, the means of assessing the

structure and properties of a general polymer will be discussed. Section 4 deals with a numerical application of the electrostatically biased polymer network. This demonstrates the influence of performing the polymerization process of a polymer under an electric field, on the structure of the network and it's properties, all while comparing it to an isotropic polymer network and to the phenomenological model. Next, our experimental work is presented in section 5, which is meant to give an additional perspective than our theoretical work. The experimental work includes an evaluation of the influence of uniaxial and biaxial stretching of DEs on their dielectric constant. Moreover, we introduce a new experimental system which allows us to evaluate the variations in the dielectric constant of DEs at different magnitudes of electric fields. Conclusions are gathered in section 6.

2 Theoretical background

(Note: Multiscale entropy based analysis)

A mechanical and electrostatic energy balance is formulated in terms of the electric enthalpy. The analyses will be carried out by taking into account the entropy of the chains network within the framework of statistical mechanics with the appropriate kinematic and energetic constraints.

2.1 Continuum electroelasticity

(Note: basic continuum mechanics - mechanics aspect)

Consider an electroelastic solid continuum in a stress-free configuration in the absence of electric field and mechanical load. Let material particles be labelled by their position vector $\mathbf{X}$ in this referential configuration. In the deformed configuration the point $\mathbf{X}$ occupies the position $\mathbf{x} = \chi(\mathbf{X}, \mathbf{t})$ where the vector field χ describes the deformation of the material. We require χ to be a one-to-one, orientation-preserving and twice continuously differentiable mapping [Dorfmann and Ogden, 2005].

(Note: continuum mechanics - mechanics)

The deformation gradient tensor is

$$\boldsymbol{F} = \nabla_{\mathbf{X}} \chi(\mathbf{X}, \mathbf{t}), \tag{1}$$

where $\nabla_{\mathbf{X}}$ is the gradient operator and the subscript $\mathbf{X}$ implies that the derivative is taken with respect to the referential coordinate system. The Cartesian components of $\boldsymbol{F}$ are $\boldsymbol{F}_{ij} = \frac{\partial \mathbf{x}_i}{\partial \mathbf{X}_j}$, where $\mathbf{X}_i$ and $\mathbf{x}_i$ $i = 1, 2, 3$, are the Cartesian components of $\mathbf{X}$ and $\mathbf{x}$, respectively. $J \equiv \det(\boldsymbol{F})$ is the ratio between volume elements in the current and reference configurations, with the convention of being strictly positive. Moreover, the velocity of the material points is $\mathbf{v}(\mathbf{x})$ and accordingly the spatial velocity gradient is

$$\mathbf{L} = \nabla_{\mathbf{x}} \mathbf{v} = \dot{\boldsymbol{F}} \boldsymbol{F}^{-1}, \tag{2}$$

where $\nabla_{\mathbf{x}}$ is the gradient operator taken with respect to the current coordinate system.

(Note: continuum mechanics - electrostatic)

The body is subjected to an electric field $\mathbf{E}(\mathbf{x})$, which satisfies the relation $\nabla_{\mathbf{x}} \times \mathbf{E}(\mathbf{x}) = 0$ in the entire space. The electric potential ϕ is a scalar quantity defined such that $\mathbf{E} = -\nabla_{\mathbf{x}} \phi$. The electric induction, also known as the electric displacement, is

$$\mathbf{D}(\mathbf{x}) = \epsilon_0 \, \mathbf{E}(\mathbf{x}) + \mathbf{P}(\mathbf{x}), \tag{3}$$

where the constant ϵ_0 is the permittivity of vacuum and $\mathbf{P}(\mathbf{x})$ is the electric dipole-density, also known as the polarization. In vacuum $\mathbf{P} = 0$. The electric displacement in ideal dielectrics or in a continuum with no free charges is governed by the equation

$$\nabla_{\mathbf{x}} \cdot \mathbf{D}(\mathbf{x}) = 0. \tag{4}$$

(Note: continuum mechanics - the electromechanical coupling)

The electrical boundary conditions for the electromechanical problem are given in terms of the electric potential or the charge per unit area on the boundary ρ_a, which is the charge on the electrodes such that $\mathbf{D} \cdot \hat{\mathbf{n}} = -\rho_a$, where $\hat{\mathbf{n}}$ is the outer pointing unit vector normal to the boundary in the current configuration. The mechanical boundary conditions are stated in terms of the displacement or the mechanical traction $\mathbf{t}$. The electric field in the surrounding space induces Maxwell's stress

$$\boldsymbol{\sigma}^M = \epsilon_0 \left(\mathbf{E} \otimes \mathbf{E} - \frac{1}{2}(\mathbf{E} \cdot \mathbf{E})\boldsymbol{I} \right). \tag{5}$$

Accordingly, the traction boundary condition is $\left(\boldsymbol{\sigma} - \boldsymbol{\sigma}^M\right) \hat{\mathbf{n}} = \mathbf{t}$. Assuming no body forces, the stress that develops in a dielectric $\boldsymbol{\sigma}$ due to the electromechanical loading satisfy the equilibrium equation

$$\nabla_{\mathbf{x}} \cdot \boldsymbol{\sigma} = 0. \tag{6}$$

(Note: The first law of thermodynamics - energy balance)

A balance of energy is formulated through the first law of thermodynamics

$$\frac{\mathrm{d}U}{\mathrm{d}t} = \frac{\mathrm{d}W}{\mathrm{d}t} + \frac{\mathrm{d}Q}{\mathrm{d}t}, \tag{7}$$

where U represents the internal energy stored in the material, W is the work of any external sources, mechanical and electrical, and Q denotes the quantity of energy suplied to the system as heat. Following McMeeking and Landis [2005], McMeeking et al. [2007] and Cohen et al. [2016], a Legendre transform of the internal energy is used in order to formulate the energy balance in terms of the electric enthalpy-density $H = U - J\mathbf{P} \cdot \mathbf{E}$. In order to formulate the energy balance in terms of entropy, which relates to the systems number of microscopic configurations, we refer to a polymer as a reversible or conservative material [McMeeking and Landis, 2005], i.e. a material that does not absorb the work done by external agents but store it as dielectric polarization or elastic deformation. Hence, following Clausius theorem in the case of a reversible material or system, the entropy change is defined as $\mathrm{d}S = \frac{\mathrm{d}Q}{T}$, where S is the entropy-density function per unit referential volume and T is the absolute temperature. Thus, while taking into account the analysis presented in appendix A [deBotton, 2020], we consider a general representation in which

the first law of thermodynamics is

$$\dot{H}^{\Upsilon} - \frac{\mathrm{d}}{\mathrm{d}t}\int_{\mathbb{R}^3} \frac{\epsilon_0}{2}\mathbf{E}\cdot\mathbf{E}\mathrm{d}V = \dot{W}^{\Upsilon} + T\dot{S}^{\Upsilon}, \tag{8}$$

where we consider an electroelastic system $\Upsilon \subset \mathbb{R}^3$.

In the work of Cohen et al. [2016], a specific representation of Eq. (8) was presented for the analysis of the energy balance in a single polymer chain

$$\frac{\mathrm{d}}{\mathrm{d}t}\int_{V_0} H\left(\boldsymbol{F},\mathbf{E}\right)\mathrm{d}V_0 - \frac{\mathrm{d}}{\mathrm{d}t}\int_{\mathbb{R}^3} \frac{\epsilon_0}{2}\mathbf{E}\cdot\mathbf{E}\mathrm{d}V = \frac{\mathrm{d}W}{\mathrm{d}t} + T\frac{\mathrm{d}}{\mathrm{d}t}\int_{V_0} S\left(\boldsymbol{F},\mathbf{E}\right)\mathrm{d}V_0, \tag{9}$$

where we consider a dielectric body that occupies the region $V_0 \subset \mathbb{R}^3$ with a boundary ∂V_0 before the deformation and the region $V \subset \mathbb{R}^3$ with a boundary ∂V after the deformation, at the current configuration.

The rate of the electric enthalpy is [Cohen and deBotton, 2014]

$$\frac{\mathrm{d}}{\mathrm{d}t}\int_{V_0} H\left(\boldsymbol{F},\mathbf{E}\right)\mathrm{d}V_0 = \int_V \frac{1}{J}\frac{\partial H\left(\boldsymbol{F},\mathbf{E}\right)}{\partial \boldsymbol{F}}\boldsymbol{F}^{\mathrm{T}} : \mathbf{L}\mathrm{d}V + \int_V \frac{1}{J}\frac{\partial H\left(\boldsymbol{F},\mathbf{E}\right)}{\partial \mathbf{E}}\cdot\dot{\mathbf{E}}\mathrm{d}V, \tag{10}$$

and the rate of entropy is

$$\frac{\mathrm{d}}{\mathrm{d}t}\int_{V_0} S\left(\boldsymbol{F},\mathbf{E}\right)\mathrm{d}V_0 = \int_V \frac{1}{J}\frac{\partial S\left(\boldsymbol{F},\mathbf{E}\right)}{\partial \boldsymbol{F}}\boldsymbol{F}^{\mathrm{T}} : \mathbf{L}\mathrm{d}V + \int_V \frac{1}{J}\frac{\partial S\left(\boldsymbol{F},\mathbf{E}\right)}{\partial \mathbf{E}}\cdot\dot{\mathbf{E}}\mathrm{d}V. \tag{11}$$

If we assume no free charges in the material and neglect body forces, the power extracted by the external mechanical and electrical agents on the system is [McMeeking and Landis, 2005, McMeeking et al., 2007, Cohen et al., 2016]

$$\frac{\mathrm{d}W}{\mathrm{d}t} = \int_{\partial V} \mathbf{t}\cdot\mathbf{v}\,\mathrm{d}A - \int_{\partial V} \rho_a\frac{\mathrm{d}\phi}{\mathrm{d}t}\,\mathrm{d}A, \tag{12}$$

which can also be formulated as [McMeeking et al., 2007]

$$\frac{\mathrm{d}W}{\mathrm{d}t} = \int_V \left(\boldsymbol{\sigma} - \boldsymbol{\sigma}^M - \mathbf{E}\otimes\mathbf{P}\right) : \mathbf{L}\mathrm{d}V - \frac{\mathrm{d}}{\mathrm{d}t}\int_{\mathbb{R}^3} \frac{\epsilon_0}{2}\mathbf{E}\cdot\mathbf{E}\mathrm{d}V - \int_V \mathbf{P}\cdot\dot{\mathbf{E}}\mathrm{d}V + \int_{\mathbb{R}^3/V} \left(\boldsymbol{\sigma} - \boldsymbol{\sigma}^M\right) : \mathbf{L}\mathrm{d}V. \tag{13}$$

By takin into account Eq. (10), Eq. (11) and Eq. (13) in Eq. (9)

$$\begin{aligned}\int_V \left(\frac{1}{J}\left(T\frac{\partial S\left(\boldsymbol{F},\mathbf{E}\right)}{\partial \mathbf{E}} - \frac{\partial H\left(\boldsymbol{F},\mathbf{E}\right)}{\partial \mathbf{E}}\right) - \mathbf{P}\right)\cdot\dot{\mathbf{E}}\mathrm{d}V + \int_{\mathbb{R}^3/V} \left(\boldsymbol{\sigma} - \boldsymbol{\sigma}^M\right) : \mathbf{L}\mathrm{d}V + \\ \int_V \left(\boldsymbol{\sigma} - \boldsymbol{\sigma}^M - \mathbf{E}\otimes\mathbf{P} - \frac{1}{J}\left(\frac{\partial H\left(\boldsymbol{F},\mathbf{E}\right)}{\partial \boldsymbol{F}} - T\frac{\partial S\left(\boldsymbol{F},\mathbf{E}\right)}{\partial \boldsymbol{F}}\right)\boldsymbol{F}^{\mathrm{T}}\right) : \mathbf{L}\mathrm{d}V = 0.\end{aligned} \tag{14}$$

As it is assumed that Eq. (14) fits every acceptable process, by following Coleman and Noll [1963] it is obtained that

$$\boldsymbol{\sigma} = \boldsymbol{\sigma}^m + \mathbf{E} \otimes \mathbf{P} + \boldsymbol{\sigma}^M, \tag{15}$$

where

$$\boldsymbol{\sigma}^m = \frac{1}{J}\left(\frac{\partial H\left(\boldsymbol{F}, \mathbf{E}\right)}{\partial \boldsymbol{F}} - T\frac{\partial S\left(\boldsymbol{F}, \mathbf{E}\right)}{\partial \boldsymbol{F}}\right)\boldsymbol{F}^{\mathrm{T}}, \tag{16}$$

is the mechanical stress [Cohen et al., 2016], and $\mathbf{E} \otimes \mathbf{P}$ is the polarizetion stress where

$$\mathbf{P} = \frac{1}{J}\left(T\frac{\partial S\left(\boldsymbol{F}, \mathbf{E}\right)}{\partial \mathbf{E}} - \frac{\partial H\left(\boldsymbol{F}, \mathbf{E}\right)}{\partial \mathbf{E}}\right). \tag{17}$$

Furthermore, when dealing with incompressible materials

$$\boldsymbol{\sigma} = \boldsymbol{\sigma}^m + \mathbf{E} \otimes \mathbf{P} + \boldsymbol{\sigma}^M + p_\star \boldsymbol{I}, \tag{18}$$

where $p_\star$ is an arbitrary Lagrange multiplier corresponding to the indeterminate hydrostatic pressure that results from the incompressibility constraint and $\boldsymbol{I}$ is the identity matrix. The corresponding deviatoric stress, which is related to shape change, is

$$\boldsymbol{\sigma}_{\mathrm{Dev}} = \boldsymbol{\sigma} - \frac{\mathrm{tr}\left(\boldsymbol{\sigma}\right)}{3}. \tag{19}$$

2.2 Entropy-driven electroelasticity of an isotropic polymer network

(Note: defining the construct and directions in the polymer)

According to the work of Cohen et al. [2016], in order to evaluate the properties and structure of different polymers the analysis starts with a single polymer chain with n dipolar monomers. The length between the two contact points of a monomer with its neighbors is l. We define a coordinate system $\left\{\hat{\mathbf{E}}, \hat{\mathbf{Y}}, \hat{\mathbf{Z}}\right\}$ (Fig. 1) as the chain is subjected to an electric field $\mathbf{E} = E\hat{\mathbf{E}}$. In this system

$$\hat{\boldsymbol{\xi}} = \cos\theta\hat{\mathbf{E}} + \sin\theta\left(\cos\phi\hat{\mathbf{Y}} + \sin\phi\hat{\mathbf{Z}}\right), \tag{20}$$

is a unit vector where $0 \leq \theta < \pi$ is the angle between $\hat{\boldsymbol{\xi}}$ and the electric field and $0 \leq \phi < 2\pi$ is the angle of its projection on the plane perpendicular to $\hat{\mathbf{E}}$ with $\hat{\mathbf{Y}}$. We define $\mathrm{d}\Gamma = \sin\theta\,\mathrm{d}\theta\,\mathrm{d}\phi$ as the differential solid angle. We also formally define that Γ varies in the range from 0 to Γ_0.

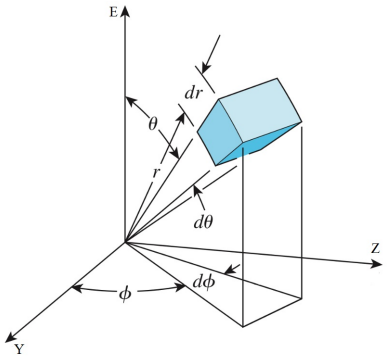

Figure 1: A schematic description of the coordinate system $\left\{\hat{\mathbf{E}}, \hat{\mathbf{Y}}, \hat{\mathbf{Z}}\right\}$ and the applied spherical coordinates.

(Note: a chain's number of possible configurations and constraints (+Stirling's approximation)**)**

The number of possible configurations of a single polymer chain is

$$\Omega^C = \frac{n!}{\Pi_i \left(n_i!\right)}, \tag{21}$$

where n_i represent the number of dipolar monomers aligned along $\hat{\boldsymbol{\xi}}$ in the range $\theta_i \leq \theta < \theta_i + \mathrm{d}\theta$ and $\phi_i \leq \phi < \phi_i + \mathrm{d}\phi$. For convenience we define that θ_i and ϕ_i correspond to the unit vector $\hat{\boldsymbol{\xi}}_i$. The entropy of the chain is

$$S^C = k\, \ln\left(\Omega^C\right) = k\, \left(n\, \ln\left(n\right) - n - \sum_i n_i \ln\left(n_i\right) + \sum_i n_i\right), \tag{22}$$

where Stirling's approximation is implemented and k is Boltzmann constant. The chain is subjected to three constraints:

$$\sum_i n_i = n, \tag{23}$$

$$\sum_i l\, n_i \hat{\boldsymbol{\xi}}_i = \mathbf{r}, \tag{24}$$

where the end-to-end vector of the monomers chain is $\mathbf{r} = r\, \hat{\mathbf{r}}$, with $\hat{\mathbf{r}} = \cos\Theta \hat{\mathbf{E}} + \sin\Theta \left(\cos\Phi \hat{\mathbf{Y}} + \sin\Phi \hat{\mathbf{Z}}\right)$, and

$$\sum_i n_i h_i = H^C, \tag{25}$$

where h_i is the electrical enthalpy of a monomer directed along $\hat{\boldsymbol{\xi}}_i$ and H^C is the enthalpy of the chain.

(Note: maximizing the entropy according to the constraints)

We assume that the polymer chain occupies the most probable configuration under

the given constraints, and therefore we are interested in maximizing the entropy,

$$S^C = k\left(\ln\left(\Omega^C\right) + \alpha\left(\sum_i n_i - n\right) + \boldsymbol{\tau}\cdot\left(\sum_i n_i\hat{\boldsymbol{\xi}}_i - \frac{\mathbf{r}}{l}\right) + \gamma\left(\sum_i n_i h_i - H^C\right)\right), \tag{26}$$

where α, $\boldsymbol{\tau}$ and $\boldsymbol{\gamma}$ are Lagrange multipliers. The derivative of S_C with respect to n_i is

$$\frac{\partial S^C}{\partial n_i} = k\left(-\ln\left(n_i\right) + \alpha + \boldsymbol{\tau}\cdot\hat{\boldsymbol{\xi}}_i + \gamma h_i\right) = 0, \tag{27}$$

from which

$$n_i = \exp\left(\alpha + \boldsymbol{\tau}\cdot\hat{\boldsymbol{\xi}}_i + \gamma h_i\right). \tag{28}$$

Upon substitution of the latter into Eq. (26), the maximum entropy that can be achieved by the chain is [Cohen et al., 2016],

$$S^C = k\left(n\,\ln\left(n\right) - \alpha\, n - \boldsymbol{\tau}\cdot\frac{\mathbf{r}}{l} - \gamma H^C\right). \tag{29}$$

(Note: Lagrange multiplier - inverse temperature)

We assume that the polymer chains do not interact with one another. Consequently, in a volume element $\mathrm{d}V_0$, the total entropy-density and the total electrical enthalpy-density function are $S = \frac{1}{\mathrm{d}V_0}\sum_k S_k^C$ and $H = \frac{1}{\mathrm{d}V_0}\sum_k H_k^C$, respectively. Accounting for the first law of thermodynamics with respect to the enthalpy of the k-th chain we obtain

$$\frac{\partial H}{\partial H_k^C} = T\frac{\partial S}{\partial H_k^C}, \tag{30}$$

from which we can derive the relation

$$\gamma = -\frac{1}{k\,T}, \tag{31}$$

where Eq. (29) is used.

(Note: PDF of a monomer according to the constraints and with maximum entropy (+calculating the rest of the Lagrange multipliers and Hc))

From the constraint Eq. (23) and Eq. (27)

$$\sum_i n_i = \exp\left(\alpha\right)\int_0^{\Gamma_0}\exp\left(\boldsymbol{\tau}\cdot\hat{\boldsymbol{\xi}} - \frac{h}{k\,T}\right)\mathrm{d}\Gamma = n, \tag{32}$$

where Eq. (29) is used and the summation is replaced by an integral over all the orientations of the monomers. Therefore,

$$\exp\left(\alpha\right) = \frac{n}{Z}, \tag{33}$$

where

$$Z = \int_0^{\Gamma_0} \exp\left(\boldsymbol{\tau}\cdot\hat{\boldsymbol{\xi}} - \frac{h}{k\,T}\right)\mathrm{d}\Gamma, \tag{34}$$

is the partition function. Subsequently, from Eq. (28) we have that

$$p\left(\hat{\boldsymbol{\xi}}, h\right) = \frac{1}{Z}\exp\left(\boldsymbol{\tau}\cdot\hat{\boldsymbol{\xi}} - \frac{h}{k\,T}\right), \tag{35}$$

is the probability density function (PDF) that a monomer is in the direction $\hat{\boldsymbol{\xi}}$ and has an electrical-enthalpy h. An implicit equation from which the Lagrange multiplier $\boldsymbol{\tau}$ is computed follows from constraint Eq. (24),

$$\int_0^{\Gamma_0} \hat{\boldsymbol{\xi}}\, p\,\mathrm{d}\Gamma = \frac{\mathbf{r}}{n\,l}. \tag{36}$$

From Eq. (25) the enthalpy of the chain is

$$\int_0^{\Gamma_0} h\, p\,\mathrm{d}\Gamma = H^C. \tag{37}$$

(Note: monomer enthalpy and different dipole types)

Following Blythe and Bloor [2005], Cohen and deBotton [2014, 2015] and Cohen et al. [2016], the electrical enthalpy of a dipole oriented along $\hat{\boldsymbol{\xi}}$ is

$$h = \mathbf{m}\cdot\mathbf{E}, \tag{38}$$

where the dipole vector $\mathbf{m}$ is determined according to a relevant model that represents the local relation. Three specific models were accounted for. The first corresponds to a spontaneous dipole or a rigid dipole with a constant magnitude [Blythe and Bloor, 2005]

$$\mathbf{m}_S = \kappa_P\hat{\boldsymbol{\xi}}. \tag{39}$$

The second model is of a uniaxial dipole whose magnitude depends on the electric field [Stockmayer, 1967]

$$\mathbf{m}_U = \kappa_U\,\hat{\boldsymbol{\xi}}\otimes\hat{\boldsymbol{\xi}}\,\mathbf{E}, \tag{40}$$

where κ_U is commonly referred to as the *polarizability* of the dipole. The third type is the transversely isotropic (TI) model [Stockmayer, 1967]

$$\mathbf{m}_{TI} = \frac{1}{2}\kappa_{TI}\left(\boldsymbol{I} - \hat{\boldsymbol{\xi}}\otimes\hat{\boldsymbol{\xi}}\right)\mathbf{E}, \tag{41}$$

where in this case the dipole is perpendicular to $\hat{\boldsymbol{\xi}}$. Note that since we do not account for the local electrostatic interactions between the dipolar monomers, the electric field induced over the monomers in the chain is uniform.

We note that in order to have that three dielectrics composed of a random and uniform distribution of spontaneous, uniaxial and transversely isotropic dipoles admit the same behavior in the limit of infinitesimal deformations and small electric fields, the relations $\kappa_U = \kappa_{TI} = \frac{\kappa_P^2}{k\,T} = \kappa$ are set. The polarizability is taken as $\kappa = \frac{3}{n_0}\,\epsilon_0\,\chi_0$ [Cohen et al., 2016], where $\chi_0 = \epsilon_r - 1$ is the initial susceptibility and ϵ_r is the relative permittivity. $n_0 = N\,n$ is the number of monomers in a unit referential volume where N is the number of chains in the unit referential volume.

(Note: PDF in the amorphous case)

In the case of an amorphous polymer the chain's constraints, presented in Eq. (23), Eq. (24) and Eq. (25), are irrelevant as there are no such limitations on a single monomer. Therefore $\boldsymbol{\tau} = 0$ and the adjusted form of the PDF in Eq. (35) is

$$p\left(\hat{\boldsymbol{\xi}}\right) = \frac{1}{Z}\,\exp\left(-\frac{h}{k\,T}\right), \tag{42}$$

where

$$Z = \int \exp\left(-\frac{h}{k\,T}\right) \mathrm{d}\Gamma, \tag{43}$$

and the enthalpy of the monomer is calculated by using Eq. (38) according to the correct dipole type.

(Note: analytical calculation - PDF in the amorphous case - U and TI)

In addition to the numerical calculations for the PDF in the amorphous case, the amorphous monomer distribution can also be calculated by the analytical analysis presented by Cohen et al. [2016], as

$$p_U = \frac{\omega}{4\pi\,D\left(\omega\right)}\,\exp\left(-\omega^2\,\sin^2\left(\theta_i\right)\right), \tag{44}$$

is the PDF of the uniaxial dipole, where $\omega = \sqrt{\frac{\kappa}{k\,T}}E = \frac{\kappa_P\,E}{k\,T}$ and $D\left(\omega\right) = \exp\left(-\omega^2\right)\int_0^\omega \exp\left(t^2\right)dt$ is the Dawson function. The PDF for the TI dipole is

$$p_{TI} = \frac{\omega}{\left(2\pi\right)^{3/2}\,\mathrm{Erf}\left(\frac{\omega}{\sqrt{2}}\right)}\,\exp\left(-\frac{\omega^2}{2}\,\cos^2\left(\theta_i\right)\right), \tag{45}$$

where $\mathrm{Erf}\left(x\right)$ is the error function.

2.3 Phenomenological approach to electroelasticity

(Note: A reference for the results in the application section)

A predictive material model, a relatively simple model that allow for reasonable assumptions, based on settings of continuum mechanics is used from the phenomenological viewpoint as a comparison to the results of our examinations. In the current work a constitutive law for the material is required to be expressed through an energy density function that depends on both the deformation and the electric displacement or the electric field. Thus, as a reference, we recall the extended neo-Hookean energy-density function for an ideal elastic dielectric (IED) [Dorfmann and Ogden, 2005]

$$W\left(\boldsymbol{F}, \mathbf{E}\right) = \frac{\mu}{2}\left(\mathrm{Tr}\Big(\boldsymbol{F}^{\mathrm{T}}\boldsymbol{F} - \boldsymbol{I}\Big)\right) + \frac{\epsilon_0\epsilon_r}{2}\mathbf{E}\cdot\mathbf{E}, \tag{46}$$

where μ is the shear modulus of the material. From Eq. (46) and on the basis of thermodynamic arguments, assuming a conservation of energy and a reversible or conservative material, the constitutive equations for an incompressible IED can be expressed as

$$\boldsymbol{\sigma} = \boldsymbol{F}\frac{\partial W}{\partial \boldsymbol{F}} + p_\star \boldsymbol{I} = \mu \boldsymbol{F}\boldsymbol{F}^{\mathrm{T}} + \mathbf{E}\otimes\mathbf{D} + p_\star \boldsymbol{I}, \tag{47}$$

and

$$\mathbf{D} = \epsilon_0\epsilon_r\mathbf{E}, \tag{48}$$

in accordance with Eq. (3) as the relative permittivity is considered to be constant. We note that, in general, this model does not accurately retrieves experimental results for coupled electromechanical loading.

3 Electroelasticity of solutions and anisotropic networks of polymer molecules

An in-depth multiscale analysis of the electromechanical coupling in DEs, which is inherented from their microstructure, is carried out. The interplay between the macroscopic deformation of the DEs and the rearrangement of the monomers in a network of polymer chains as a result of external electrical and mechanical loading will be examined.

3.1 First law of thermodynamics

The first law of thermodynamics, presented in Eq. (8), is formulated as a general representation for the electromechanical situation. Such representation accounts for the conservation of energy of a body that is subjected to an electric field while allowing us to formulate the energy balance in terms of the electric enthalpy and the entropy of the system.

For systematic analysis of the electromechanical coupling in polymers, from the microscopic to the macroscopic levels, we specialize Eq. (8) to five different systems. The simplest ones are based on the system presented in Fig. 2 which is essentially a one dimensional system. Subsequently we examine a network that is treated as a 3 D body.

3.2 1 D systems of charge, dipole and molecular chains in electric field

In a 1 D system (see Fig. 2), we define the vector connecting the two ends (i.e. the end-to-end vector of the system) as $\mathbf{r} = \mathbf{r}_- - \mathbf{r}_+$. $\mathbf{f}^{+/-}$, $\mathbf{V}^{+/-}$ and $Q^{+/-}$ are the forces, velocities and charges on the system's boundaries, respectively. The rate of enthalpy and the rate of entropy are $\dot{H}^{\Upsilon} = \dot{H}(\mathbf{r}, \mathbf{E}_0)$ and $\dot{S}^{\Upsilon} = \dot{S}(\mathbf{r}, \mathbf{E}_0)$, respectively. The power extracted by the external agents (Eq. (12)) is $\dot{W}^{\Upsilon} = \sum \mathbf{f} \cdot \mathbf{V} + \sum Q\dot{\phi}$.

3.2.1 A single electric charge

We begin with an analysis of the second term in Eq. (8), that concerns the variation in the energy of the system due to variations in the electric field generated by a single charge. To be precise, the present case describes a 0 D system.

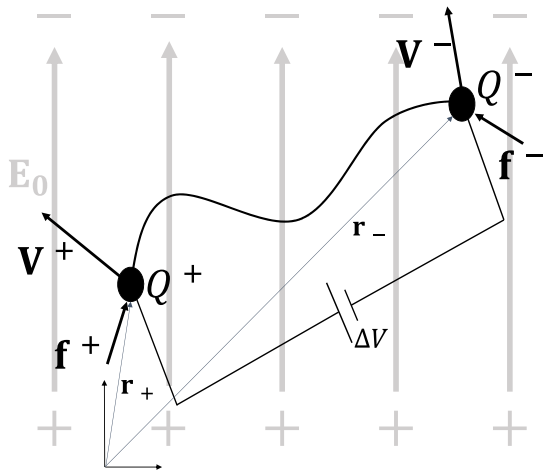

Figure 2: Schematic description of an arbitrary one dimensional system subjected to electromechanical exitation at its boundary.

The electric field due to a particle with a constant electric charge Q is derived from Coulomb's law as

$$\mathbf{E}^{Q}(\mathbf{g}) = \frac{Q\hat{\mathbf{g}}}{4\pi\epsilon_0 g^2}, \tag{49}$$

where in the current case $\mathbf{g} = g\hat{\mathbf{g}}$ is the vector from a specific point in space to the charge's location. Thus, as electric fields satisfy the superposition principle, the total electric field at the mentioned location is

$$\mathbf{E}(\mathbf{g}) = \mathbf{E}_0 + \mathbf{E}^{Q}(\mathbf{g}) = \mathbf{E}_0 + \frac{Q\hat{\mathbf{g}}}{4\pi\epsilon_0 g^2}, \tag{50}$$

where $\mathbf{E}_0 = E_0\,\hat{\mathbf{E}}$ is the electric field subjected on the entire space. Accordingly, the second term in Eq. (8) is

$$\begin{aligned} &\frac{\epsilon_0}{2}\frac{\mathrm{d}}{\mathrm{d}t}\int_{\mathbb{R}^3}\left(\mathbf{E}_0\cdot\mathbf{E}_0 + 2\frac{Q\mathbf{E}_0\cdot\hat{\mathbf{g}}}{4\pi\epsilon_0 g^2} + \frac{Q\hat{\mathbf{g}}}{4\pi\epsilon_0 g^2}\cdot\frac{Q\hat{\mathbf{g}}}{4\pi\epsilon_0 g^2}\right)\mathrm{d}V \\ =&\frac{\epsilon_0}{2}\frac{\mathrm{d}}{\mathrm{d}t}\int_{\mathbb{R}^3}\left(\mathbf{E}_0\cdot\mathbf{E}_0 + \frac{Q\mathbf{E}_0\cdot\hat{\mathbf{g}}}{2\pi\epsilon_0 g^2} + \frac{Q^2}{16\pi^2\epsilon_0^2 g^4}\right)\mathrm{d}V. \end{aligned} \tag{51}$$

We note that the first and third terms in Eq. (51) are constants. Moreover, for any spherical region about the charge with inner radius R_i and outer radius R_o the variation in the energy depends on

$$\frac{Q}{4\pi}\int_0^{2\pi}\int_0^{\pi}\int_{R_i}^{R_o}\frac{\mathbf{E}_0\cdot\hat{\mathbf{g}}}{g^2}\mathbf{g}^2\sin\Theta\mathrm{d}g\mathrm{d}\Theta\mathrm{d}\Phi = \frac{QE_0}{2}\frac{\mathrm{d}}{\mathrm{d}t}\int_{R_i}^{R_o}\mathrm{d}g\int_0^{\pi}\cos\Theta\sin\Theta\mathrm{d}\Theta \equiv 0, \tag{52}$$

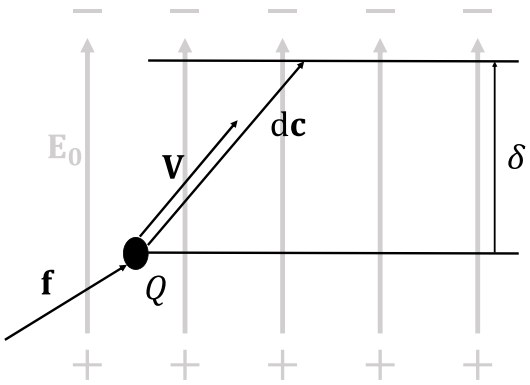

Figure 3: Schematic description of a single charge subjected to an electric field.

where according to Eq. (20) $\mathbf{E}_0 \cdot \hat{\mathbf{g}} = E_0 \cos\Theta$. Since this integral vanishes identically, so does its time derivative. Thus, for any motion of a single charge in a uniform electric field the second term in Eq. (8) vanishes.

Taking into account Eq. (52) and neglecting the enthalpy and entropy, as we assume no material, Eq. (8) is reduced to $\dot{W} = 0$. Thus, by observing Fig. 3 and from Eq. (12) for a single charge

$$\dot{W} = \mathbf{f} \cdot \frac{\mathrm{d}\mathbf{c}}{\mathrm{d}t} - Q\frac{\mathrm{d}\phi}{\mathrm{d}t} = 0, \tag{53}$$

where $\mathbf{c}$ denote the location of the charge. The velocity of the charge is $\mathbf{V} = \frac{\mathrm{d}\mathbf{c}}{\mathrm{d}t}$ where $\mathrm{d}\mathbf{c} = \delta\hat{\mathbf{E}} + \mathrm{d}\mathbf{c}_T$ represent the change in the location of the charge during $\mathrm{d}t$, $\mathrm{d}\phi = -\mathbf{E}_0 \cdot \mathrm{d}\mathbf{c} = -\delta E_0$ and $\mathbf{f} = f_E\hat{\mathbf{E}} + \mathbf{f}_T$. Moreover, $\mathrm{d}\mathbf{c}_T$ and $\mathbf{f}_T$ are the components of $\mathrm{d}\mathbf{c}$ and $\mathbf{f}$, respectively, that are perpendicular to the direction $\hat{\mathbf{E}}$. Thus,

$$\dot{W} = \frac{\mathrm{d}}{\mathrm{d}t}\left(\mathbf{f} \cdot \mathrm{d}\mathbf{c} + Q\delta E_0\right) = \frac{\mathrm{d}}{\mathrm{d}t}\left(f_E\delta + \mathbf{f}_T \cdot \mathrm{d}\mathbf{c}_T + Q\delta E_0\right) = 0. \tag{54}$$

Therefore, since in an equilibrium state Eq. (54) equals zero and $\mathrm{d}\mathbf{c}_T$ is arbitrary, we conclude that $\mathbf{f}_T \equiv 0$ and $f_E = -QE_0$. This is precisely Coulomb's force on a charge of magnitude Q in an electric field $\mathbf{E}_0$.

3.2.2 Dipoles

Consider a charged nonpolarized rigid dipole and, as in the previous case, we assume no material and neglect the enthalpy and entropy. As can be seen in Fig. 4, the dipole is described as two charges, Q^+ and Q^-, connected by a stiff rod with length l and in the direction of the unit vector $\hat{\boldsymbol{\xi}}$. We assume that $Q^+ = -Q^- = Q$.

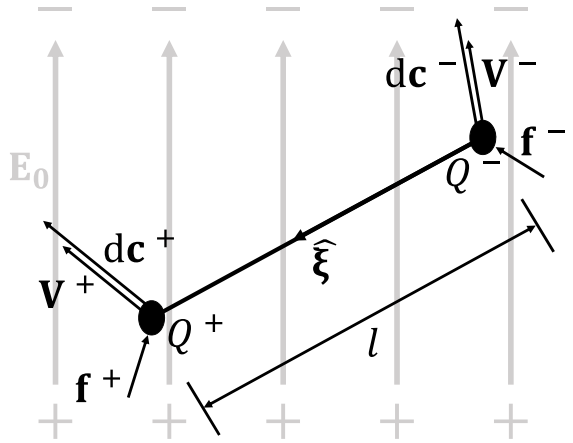

Figure 4: Schematic description of a single dipole consisting of two charges, Q^+ and Q^-, connected by a stiff rod in an electric field.

Again, we begin with an analysis of the second term in Eq. (8), the variation in the energy of the system due to variations in the electric field generated by both the charges. Hence, in accordance with the superposition principle

$$\begin{aligned}\mathbf{E} &= \mathbf{E}_0 + \mathbf{E}^{Q^+}\left(\mathbf{g}^+\right) - \mathbf{E}^{Q^-}\left(\mathbf{g}^-\right) = \mathbf{E}_0 + \frac{Q\hat{\mathbf{g}}^+}{4\pi\epsilon_0\left(g^+\right)^2} - \frac{Q\hat{\mathbf{g}}^-}{4\pi\epsilon_0\left(g^-\right)^2}, \\ &= \mathbf{E}_0 + \mathbf{E}^+ + \mathbf{E}^-, \end{aligned} \tag{55}$$

where $\mathbf{g}^+ = g^+\hat{\mathbf{g}}^+$ and $\mathbf{g}^- = g^-\hat{\mathbf{g}}^-$ are the vectors from a specific point in space to the locations of the charges Q^+ and Q^-, respectively. Accordingly, the second term in Eq. (8) is

$$\frac{\epsilon_0}{2}\frac{\mathrm{d}}{\mathrm{d}t}\int_{\mathbb{R}^3}\left(\mathbf{E}_0\cdot\mathbf{E}_0 + 2\left(\mathbf{E}_0\cdot\mathbf{E}^+ + \mathbf{E}_0\cdot\mathbf{E}^- + \mathbf{E}^+\cdot\mathbf{E}^-\right) + \mathbf{E}^+\cdot\mathbf{E}^+ + \mathbf{E}^-\cdot\mathbf{E}^-\right)\mathrm{d}V \tag{56}$$

where according to Eq. (52) the integrals of $\mathbf{E}_0\cdot\mathbf{E}^+$ and $\mathbf{E}_0\cdot\mathbf{E}^-$ vanishes identically and the rest of the terms are constants. Hence, Eq. (56) equals zero.

Thus, Eq. (8) is again reduced to $\dot{W} = 0$. From the definition of the electric potential, $\mathrm{d}\phi = -\mathbf{E}_0\cdot\mathrm{d}\mathbf{c}$. Thus, $\dot{\phi}^{+/-} = -\mathbf{E}_0\cdot\mathbf{V}^{+/-}$ and the rate of work of the external sources is

$$\dot{W} = \mathbf{f}^+\cdot\mathbf{V}^+ + \mathbf{f}^-\cdot\mathbf{V}^- + \mathbf{E}_0\cdot\left(Q^+\mathbf{V}^+ + Q^-\mathbf{V}^-\right) = 0. \tag{57}$$

Since $\mathbf{c}^+ = \mathbf{c}^- + l\hat{\boldsymbol{\xi}}$ from the geometric relation, then $\mathbf{V}^+ = \mathbf{V}^- + l\dot{\hat{\boldsymbol{\xi}}}$ and the corresponding rate of work is

$$\dot{W} = \left(\mathbf{f}^+ + \mathbf{f}^-\right)\cdot\mathbf{V}^- + l\left(\mathbf{f}^+ + Q\mathbf{E}_0\right)\cdot\dot{\hat{\boldsymbol{\xi}}} = 0. \tag{58}$$

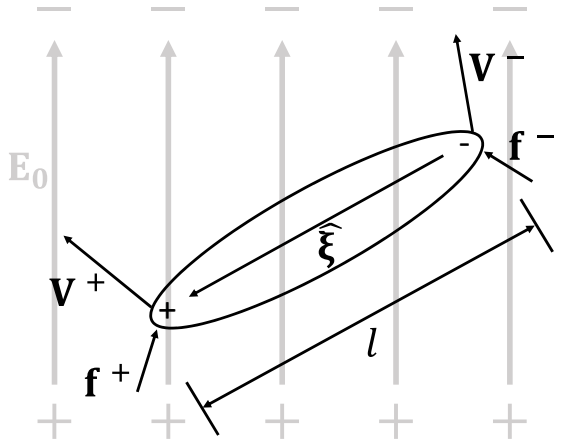

Figure 5: Schematic description of a dipole in an electric field.

Since the dipole is rigid, there is a constraint along the direction of the dipole. Thus, the forces and the electric field are splitted to components in accordance with the orthogonal system $\left\{\hat{\boldsymbol{\xi}}, \hat{\mathbf{u}}, \hat{\mathbf{s}}\right\}$ where $\hat{\mathbf{s}} = \hat{\boldsymbol{\xi}} \times \hat{\mathbf{E}}$ is perpendicular to the plane spanned by the electric field and the dipole. $\hat{\mathbf{u}} = \hat{\mathbf{s}} \times \hat{\boldsymbol{\xi}}$ is perpendicular to the dipole and is on the described plane. Hence, let $\mathbf{f}^+ = a^+\hat{\boldsymbol{\xi}} + b^+\hat{\mathbf{u}} + c^+\hat{\mathbf{s}}$, $\mathbf{f}^- = a^-\hat{\boldsymbol{\xi}} + b^-\hat{\mathbf{u}} + c^-\hat{\mathbf{s}}$ and $\mathbf{E}_0 = e\hat{\boldsymbol{\xi}} + g\hat{\mathbf{u}}$. Consequently, Eq. (58) yields

$$\dot{W} = \left(\left(a^+ + a^-\right)\hat{\boldsymbol{\xi}} + \left(b^+ + b^-\right)\hat{\mathbf{u}} + \left(c^+ + c^-\right)\hat{\mathbf{s}}\right)\cdot\mathbf{V}^- + l\left(a^+\hat{\boldsymbol{\xi}} + b^+\hat{\mathbf{u}} + c^+\hat{\mathbf{s}} + Q\left(e\hat{\boldsymbol{\xi}} + g\hat{\mathbf{u}}\right)\right)\cdot\dot{\hat{\boldsymbol{\xi}}} = 0. \tag{59}$$

Since at equilibrium Eq. (59) equals zero and $\mathbf{V}^-$ and $\dot{\hat{\boldsymbol{\xi}}}$ are arbitrary, it can be inferred from the first term that $a^+ = -a^-$, $b^+ = -b^-$ and $c^+ = -c^-$. Though, when considering the second term, we can deduce that $c^+ = 0$. Moreover, since $\dot{\hat{\boldsymbol{\xi}}} \perp \hat{\boldsymbol{\xi}}$ the dot product of the component which is along the dipole with the temporal derivative of the dipole vanishes identically. Thus, the second term of Eq. (59) does not contribute a constraint for the components of the forces in the dipole direction and $b^+ = -gQ$. These results are analogous to the requirement that the sum of the moments on the dipole vanishes.

In the case of a spontaneous and polarizable dipolar monomers (Fig. 5) the electrical enthalpy must be taken into account. According to Cohen et al. [2016], the electrical enthalpy of a dipole is

$$h = -\mathbf{m}\cdot\mathbf{E}_0, \tag{60}$$

where $\mathbf{m}$ is the dipole vector. In the case of a spontaneous dipole with a constant magnitude κ, $\mathbf{m} = \kappa\hat{\boldsymbol{\xi}}$. Hence, the electrical enthalpy is $h = -\kappa\hat{\boldsymbol{\xi}}\cdot\mathbf{E}_0$ and the rate of the

electrical enthalpy is

$$\dot{h} = -\kappa\dot{\hat{\boldsymbol{\xi}}} \cdot \mathbf{E}_0. \tag{61}$$

In this case Eq. (8) is reduced to

$$\dot{h} = \dot{W}. \tag{62}$$

Substituting Eq. (58) and Eq. (61) into Eq. (62) yields

$$-\kappa\dot{\hat{\boldsymbol{\xi}}} \cdot \mathbf{E}_0 = \mathbf{f}^+ \cdot \mathbf{V}^+ + \mathbf{f}^- \cdot \mathbf{V}^- = \left(\mathbf{f}^+ + \mathbf{f}^-\right) \cdot \mathbf{V}^- + l\mathbf{f}^+ \cdot \dot{\hat{\boldsymbol{\xi}}}, \tag{63}$$

which yields that

$$\left(\mathbf{f}^+ + \mathbf{f}^-\right) \cdot \mathbf{V}^- + \left(l\mathbf{f}^+ + \kappa\mathbf{E}_0\right) \cdot \dot{\hat{\boldsymbol{\xi}}} = 0. \tag{64}$$

Again, the forces and the electric field are splitted to components in accordance with the orthogonal system $\left\{\hat{\boldsymbol{\xi}}, \hat{\mathbf{u}}, \hat{\mathbf{s}}\right\}$, where $\mathbf{f}^+ = a^+\hat{\boldsymbol{\xi}} + b^+\hat{\mathbf{u}} + c^+\hat{\mathbf{s}}$, $\mathbf{f}^- = a^-\hat{\boldsymbol{\xi}} + b^-\hat{\mathbf{u}} + c^-\hat{\mathbf{s}}$ and $\mathbf{E}_0 = e\hat{\boldsymbol{\xi}} + g\hat{\mathbf{u}}$. Accordingly, Eq. (58) yields

$$\left(\left(a^+ + a^-\right)\hat{\boldsymbol{\xi}} + \left(b^+ + b^-\right)\hat{\mathbf{u}} + \left(c^+ + c^-\right)\hat{\mathbf{s}}\right)\cdot\mathbf{V}^- + \left(l\left(a^+\hat{\boldsymbol{\xi}} + b^+\hat{\mathbf{u}} + c^+\hat{\mathbf{s}}\right) + \kappa\left(e\hat{\boldsymbol{\xi}} + g\hat{\mathbf{u}}\right)\right)\cdot\dot{\hat{\boldsymbol{\xi}}} = 0. \tag{65}$$

Thus, as $\mathbf{V}^-$ and $\dot{\hat{\boldsymbol{\xi}}}$ are arbitrary, the first term leads us to the constraints $a^+ = -a^-$, $b^+ = -b^-$ and $c^+ = -c^-$. The second term leads to $c^+ = 0$ and since $\dot{\hat{\boldsymbol{\xi}}} \perp \hat{\boldsymbol{\xi}}$ the second term does not contribute an additional constraint on the components of the forces in the dipole direction and $b^+ = -g\frac{\kappa}{l}$. In the case where $b^+ = 0$ then $\mathbf{E}_0 \cdot \dot{\hat{\boldsymbol{\xi}}} = 0$ for equilibrium. Since $\dot{\hat{\boldsymbol{\xi}}} \perp \hat{\boldsymbol{\xi}}$ it inferes that for this specific case $\hat{\boldsymbol{\xi}} \parallel \mathbf{E}_0$. Which means that the electric field will not induce rotation on the dipole and the dipole can be at rest without application of external forces.

3.2.3 Polymer molecule (chain)

As was established, while $\frac{\mathrm{d}}{\mathrm{d}t}\int_{\mathbb{R}^3}\mathbf{E}\cdot\mathbf{E}\mathrm{d}V$ vanishes identically and whenever $\dot{W} = 0$, Eq. (8) is reduced to

$$\dot{H} = T\dot{S}. \tag{66}$$

Thus, since $T\dot{S}^C - \dot{H}^C = 0$ describes an equilibrium state for a polymer chain, it means that the preferred state of a chain can be described by determining $\max\left\{TS^C - H^C\right\}$. By taking Eq. (29) into account, the most probable state is the one that satisfies

$$\max\left\{Tk\left(n\ln(n) - \alpha\, n - \boldsymbol{\tau}\cdot\frac{\mathbf{r}}{l}\right) - (Tk\gamma + 1)\,H^C\right\}, \tag{67}$$

where from Eq. (25) $H^C(\mathbf{r},\mathbf{E}_0) = \sum_{i=1}^{n} h_i\left(\hat{\boldsymbol{\xi}}_i,\mathbf{E}_0\right)$. Furthermore, we emphasize that the analysis is executed with the assumption that r, the end-to-end length of the chain with maximum permutations (i.e. the most probable), is the only end-to-end length of chains in the direction of $\hat{\mathbf{r}}$.

(Note: The "length" of a polymer chain - general)

In order to determine the most probable r for a specific chain, the number of possible permutations is calculated for all possible end-to-end lengths in the range $0 \le r \le n\,l$. This assessment is performed for chains in all possible orientations relative to the direction of the electric field, $0 \le \Theta < \pi$. Thus, we can assess the most probable chain configuration, depending on the magnitude of the electric field in the polymerization process and the chain's inclination to the electric field.

(Note: The "length" of a polymer chain in the case of E=0 - purely mechanical case)

When examining $\mathbf{r}$ of a single polymer chain in the case of $\mathbf{E}_0 = 0$, then $H^C(\mathbf{r},0) = 0$ and the entropy of the chain is governing its behavior. By using the implicit equation from which the Lagrange multiplier $\boldsymbol{\tau}$ is computed and the probability density function that a monomer is in the direction $\hat{\boldsymbol{\xi}}$, Eq. (36) and Eq. (35) respectively, we obtain

$$\frac{\int_0^{\Gamma_0} \hat{\boldsymbol{\xi}} \exp\left(\boldsymbol{\tau}\cdot\hat{\boldsymbol{\xi}}\right) \mathrm{d}\Gamma}{\int_0^{\Gamma_0} \exp\left(\boldsymbol{\tau}\cdot\hat{\boldsymbol{\xi}}\right) \mathrm{d}\Gamma} = \frac{\mathbf{r}}{n\,l}. \tag{68}$$

Let $\boldsymbol{\tau} = a\hat{\mathbf{r}} + b\hat{\mathbf{m}}$ where $\hat{\mathbf{m}} = \frac{\mathbf{m}}{m}$ and $\mathbf{m} = \boldsymbol{\tau} - (\boldsymbol{\tau}\cdot\hat{\mathbf{r}})\,\hat{\mathbf{r}}$ in an orthogonal system $\{\hat{\mathbf{r}},\hat{\mathbf{m}},\hat{\mathbf{s}}\}$ where $\hat{\mathbf{s}} = \hat{\mathbf{r}}\times\hat{\mathbf{m}}$. In this system take $\hat{\boldsymbol{\xi}} = \cos\theta\hat{\mathbf{r}} + \sin\theta\,(\cos\phi\hat{\mathbf{m}} + \sin\phi\hat{\mathbf{s}})$, and subsequently $\boldsymbol{\tau}\cdot\hat{\boldsymbol{\xi}} = a\cos\theta + b\sin\theta\cos\phi$.

Multiplying Eq. (68) by $\hat{\mathbf{m}}$ we obtain

$$\frac{1}{Z}\int_0^{\Gamma_0} \left(\hat{\boldsymbol{\xi}}\cdot\hat{\mathbf{m}}\right)\exp\left(\boldsymbol{\tau}\cdot\hat{\boldsymbol{\xi}}\right)\mathrm{d}\Gamma = 0, \tag{69}$$

or explicitly

$$\frac{1}{Z}\int_0^{2\pi}\int_0^{\pi} \exp\left(a\,\cos\theta\right)\exp\left(b\,\sin\theta\cos\phi\right)\sin\theta\,\cos\phi\,\left(\sin\theta\,\mathrm{d}\theta\,\mathrm{d}\phi\right) = 0. \tag{70}$$

We note that the choice $b = 0$ leads to

$$\frac{1}{Z}\int_0^{\pi} \exp\left(a\,\cos\theta\right)\sin^2\theta\,\mathrm{d}\theta\int_0^{2\pi}\cos\phi\,\mathrm{d}\phi = 0, \tag{71}$$

and hence to the fulfilment of Eq. (69).

Next, by multiplying the left hand side of Eq. (68) by $\hat{\mathbf{r}}$ we obtain

$$\frac{1}{Z}\int_0^{\Gamma_0}\left(\hat{\boldsymbol{\xi}}\cdot\hat{\mathbf{r}}\right)\exp\left(\boldsymbol{\tau}\cdot\hat{\boldsymbol{\xi}}\right)\,\mathrm{d}\Gamma=\frac{1}{Z}\int_0^{2\pi}\int_0^{\pi}\exp\left(a\,\cos\theta\right)\,\cos\theta\,\sin\theta\,d\theta\,\mathrm{d}\phi. \tag{72}$$

A change of variables to $x=\cos\theta$ leads to the expression

$$\frac{\int_{-1}^{1}\exp\left(a\,x\right)\,x\,\mathrm{d}x}{\int_{-1}^{1}\exp\left(a\,x\right)\,\mathrm{d}x}=\frac{r}{n\,l}, \tag{73}$$

which can be integrated to

$$\frac{\exp\left(a\right)+\exp\left(-a\right)}{\exp\left(a\right)-\exp\left(-a\right)}-\frac{1}{a}\equiv\mathcal{L}\left(a\right)=\frac{r}{n\,l}, \tag{74}$$

where $\mathcal{L}$ is the Langevin function. Accordingly,

$$a=\mathcal{L}^{-1}\left(\frac{r}{n\,l}\right), \tag{75}$$

where $\mathcal{L}^{-1}$ is the inverse Langevin function. Note that if $\frac{r}{n\,l}\lll 1$ then $a\cong\frac{3r}{n\,l}$ and in the limit $r\to n\,l$ then $a\to\infty$.

Substituting the expression for S^C following Eq. (22) and Eq. (26)

$$\begin{aligned}\ln\left(\Omega^C\right)&=n\,\ln\left(n\right)-\sum_i n_i\ln\left(n_i\right) \qquad (76)\\ &=n\left\{\ln\left(n\right)-\frac{1}{Z}\left[\ln\left(\frac{n}{Z}\right)\int_0^{\Gamma_0}\exp\left(a\,\cos\theta\right)\,\mathrm{d}\Gamma+a\int_0^{\Gamma_0}\exp\left(a\,\cos\theta\right)\cos\theta\,\mathrm{d}\Gamma\right]\right\},\end{aligned}$$

where, from Eq. (72)

$$\int_0^{\Gamma_0}\exp\left(a\,\cos\theta\right)\cos\theta\,\mathrm{d}\Gamma=\frac{r}{n\,l}\int_0^{\Gamma_0}\exp\left(a\,\cos\theta\right)\,\mathrm{d}\Gamma, \tag{77}$$

and thus,

$$\begin{aligned}\ln\left(\Omega^C\right)&=n\left\{\ln\left(n\right)-\frac{1}{Z}\left[\left(\ln\left(\frac{n}{Z}\right)+\frac{a\,r}{n\,l}\right)\int_0^{\Gamma_0}\exp\left(a\,\cos\theta\right)\,\mathrm{d}\Gamma\right]\right\}\\ &=n\,\ln\left(Z\right)-a\frac{r}{l}. \qquad (78)\end{aligned}$$

We note that

$$Z=\frac{2\pi}{a}\left(\exp\left(a\right)-\exp\left(-a\right)\right), \tag{79}$$

and hence

$$\ln\left(\Omega^C\right) = n\,\ln\left(\frac{2\pi}{a}\left(\exp\left(a\right)-\exp\left(-a\right)\right)\right) - a\frac{r}{l}. \tag{80}$$

Note that in the limit $r \to 0$, $\ln\left(\Omega^S\right) = n\,\ln\left(4\pi\right)$ and hence $\Omega^S = (4\pi)^n$, and in the limit $r \to n\,l$, $\ln\left(\Omega^{n\,l}\right) = n\,\ln\left(\frac{2\pi}{a}\exp\left(a\right)\right) - a\,n = n\,\ln\left(\frac{2\pi}{a}\right)$ and hence $\Omega^{n\,l} = \left(\frac{2\pi}{a}\right)^n \to 0$ since $a \to \infty$. The total number of permutations of chains with end-to-end length r, as $\mathbf{E}_0 = 0$, is

$$\Omega^O\left(r\right) = 4\pi r^2\Omega^C\left(r\right) = 4\pi n^2 l^2\eta^2\Omega^C \tag{81}$$

where $\eta \equiv \frac{r}{n\,l}$. Since at $r \to 0$ Ω^S is finite then $\Omega^O\left(0\right) \to 0$ and since at $r \to n\,l$ $\Omega^S \to 0$ and r^2 is finite $\Omega^O\left(n\,l\right) \to 0$. This suggests that in the range $0 < r < n\,l$ Ω^O has a maximum.

Determination of the maximum is performed as

$$\frac{\mathrm{d}\ln\Omega^C}{\mathrm{d}\eta} = \frac{\partial\ln\Omega^C}{\partial a}\frac{\mathrm{d}a}{\mathrm{d}\eta} + \frac{\partial\ln\Omega^C}{\partial\eta}, \tag{82}$$

when treating a and η as independent variables. It can be seen from Eq. (74) and Eq. (80) that

$$\begin{aligned}\frac{\partial\ln\Omega^C}{\partial a} &= n\left(\frac{\exp\left(a\right)+\exp\left(-a\right)}{\exp\left(a\right)-\exp\left(-a\right)} - \frac{1}{a}\right) - \frac{r}{l}\\ &= n\left(\frac{\exp\left(a\right)+\exp\left(-a\right)}{\exp\left(a\right)-\exp\left(-a\right)} - \frac{1}{a}\right) - n\eta = 0,\end{aligned} \tag{83}$$

thus,

$$\frac{\mathrm{d}\ln\Omega^C}{\mathrm{d}\eta} = -a\,n. \tag{84}$$

From the distribution in the case of $\mathbf{E}_0 = 0$ (seen in Eq. (81)), as $4\pi n^2 l^2 = k$

$$\frac{1}{k}\frac{\partial\Omega^O}{\partial\eta} = 2\eta\Omega^C + \eta^2\frac{\mathrm{d}\Omega^C}{\mathrm{d}\eta} = \eta\exp\left(\ln\Omega^C\right)\left[2-\eta\,a\,n\right] = 0, \tag{85}$$

therefrom $a = \frac{2}{n\,\eta}$ or $\eta = \mathcal{L}\left(\frac{2}{n\,\eta}\right) = \coth\left(\frac{2}{n\,\eta}\right) - \frac{n\,\eta}{2}$. If n is a large number $\coth\left(\frac{2}{n\,\eta}\right) = \frac{n\,\eta}{2} + \frac{2}{3n\,\eta} + o\left(\frac{2}{n\,\eta}\right)^3$. Hence, up to a second order in $\frac{1}{n}$ $\eta = \sqrt{\frac{2}{3}}\frac{1}{\sqrt{n}} \sim \frac{0.816}{\sqrt{n}}$. This result differ from the assessment given from random walk statistics presented and used by Kuhn [1934], Treloar [1973], Arruda and Boyce [1993] and Cohen et al. [2016] but coincide with the assessed end-to-end chain length determined in Flory [1949] , Flory [1953] and Treloar [1975].

(Note: force in a single chain with no electric field)

Furthermore, the most probable end-to-end length of a chain whose one end is at the origin and the other end is located within a small $\mathrm{d}V = r^2\mathrm{d}r\mathrm{d}\phi\mathrm{d}\theta$ when a given force

$\mathbf{f} \parallel \mathbf{r}$ is acting upon it is also examined in the case of no electric field. By specializing Eq. (8) to the case of a single chain without an electric field we receive

$$\dot{W} + T\dot{S}^O(\mathbf{r}) = 0. \tag{86}$$

For this case, we define that $\mathbf{r} = \rho\mathbf{R}$, where ρ is the stretch magnitude, $\mathbf{R}$ is the end-to-end vector in the referential state of the chain and it is assumed that $\mathbf{r} \parallel \mathbf{R}$. Thus, in accordance with Eq. (22) and Eq. (81), the rate of entropy is

$$\dot{S}^O(\mathbf{r}) = \frac{\mathrm{d}S^O}{\mathrm{d}\rho}\dot{\rho} = k\left(\frac{2}{\rho} - \frac{\tau \cdot \mathbf{R}}{l}\right)\dot{\rho}, \tag{87}$$

and the rate of work of the external sources is

$$\dot{W} = \mathbf{f} \cdot \mathbf{v} = \mathbf{f} \cdot \mathbf{R}\dot{\rho}, \tag{88}$$

where $\mathbf{v} = \dot{\mathbf{r}}$, $\mathbf{f}$ is the external force operating on the chain and body forces are neglected. Substituting Eq. (87) and (88) into Eq. (86) yields

$$\begin{aligned}\left(\mathbf{f} \cdot \mathbf{R} + T\,k\left(\frac{2}{\rho} - \frac{\tau \cdot \mathbf{R}}{l}\right)\right)\dot{\rho} &= \left(\mathbf{f} \cdot \mathbf{R}\rho + T\,k\left(2 - \frac{\tau \cdot \mathbf{R}\rho}{l}\right)\right)\dot{\rho} \\ &= \left(\mathbf{f} \cdot \mathbf{r} + T\,k\left(2 - \eta\,\tau\,n\right)\right)\dot{\rho} = 0,\end{aligned} \tag{89}$$

thus,

$$\mathbf{f} = -\frac{T\,k\left(2 - \eta\,\tau\,n\right)}{r^2}\mathbf{r} = -\frac{T\,k\left(2 - \frac{r}{nl}\,\mathcal{L}^{-1}\left(\frac{r}{nl}\right)\,n\right)}{r}\hat{\mathbf{r}}, \tag{90}$$

where Eq. (75) is taken into account. Hence, in accordance with Eq. (85), when $\frac{r}{nl} = \sqrt{\frac{2}{3}}\frac{1}{\sqrt{n}}$ then $\mathbf{f} = 0$.

3.3 Polymer molecules (chains) in electric field

We examine a method for controlling the electroelastic moduli of a network. Specifically, we examine the consequence of executing the polymerization process under electric field. To this end we assume that the chains are in a solution during the polymerization. The current step assumes that the monomers are already bonded into chains, but before the curing and the toughening or hardening of the network by cross-linking of the chains. In this case we can refer to the chains as "floating" in the solution such that no external work is applied at their ends. Furthermore, we assume no interactions between the chains and determine their most probable permutations seperetly.

In accordance with the mentioned assumptions, each chain will be examined individ-

ually as the end-to-end length of a chain is $r_j = r(\Theta_j, \mathbf{E}_0)$ and the end-to-end direction of the chain is $\hat{\mathbf{r}}_j = \hat{\mathbf{r}}(\Theta_j, \Phi_j)$. According to the coordinate in Fig. 1, Θ_j is the inclination of the chains end-to-end vector relative to the direction of the electric field. Hence, as described in section 3.2.3, the suitable r_j for each Θ_j is the one that satisfies Eq. (67). In the case where $E = 0$ it is sufficient to analyze a single chain (detailed in section 3.2.3) since in this case the polymer has no preferred direction and the network is isotropic.

3.3.1 Monomers orientational distribution

(Note: calculating monomer orientations)

After calculating the polymers end-to-end chain length in each group, the orientation of the chains building blocks, the monomers, can be evaluated. The monomer orientations are investigated as a part of a chain while taking into account the suitable constraints, seen in Eq. (23), Eq. (24) and Eq. (25).

Once the end-to-end chains lengths with the maximum possible permutations are determined, i.e. the most probable end-to-end chain length for each group is found, the monomers distribution can be calculated for each chain by using Eq. (35). The probabilities for all possible orientations of the monomers are calculated in order to determine the monomers distribution of the most probable chains, found in the previous section. The mentioned orientations include all combinations of $0 \leq \theta < \pi$ and $0 \leq \phi < 2\pi$.

After obtaining the monomers orientations for each of the chain groups, a comparison can be made to the monomer distribution in the amorphous case. Such distribution can be calculated according to Eq. (42) while taking into account the correct type of dipole. Analytical approximations of the PDF in the amorphous are presented in Eq. (44) and Eq. (45) for uniaxial dipoles and transversely isotropic dipoles, respectively [Cohen et al., 2016].

3.4 An anisotropic network of polymer molecules

According to Flory [1949] the total number of internal configurations of a polymer with N polymer chains is

$$\Omega^t = N! \prod_q \left(\frac{(\omega_q)^{N_q}}{N_q!} \right), \tag{91}$$

where ω_q and N_q are the number of configurations and the number of chains associated with specific end-to-end vector, respectively. Assume, in a way of an example, that we can a-priori split the chains population into two popultions such that for all the end-to-end vectors in the two groups the number of possible configurations are ω_1 and ω_2, and the

number of chains in each group are N_1 and N_2. There are total ψ_1 and ψ_2 end-to-end vectors in the two groups such that $\psi_1 N_1 + \psi_2 N_2 = N$. Accordingly

$$\Omega^t = N! \left(\prod_{q_1=1}^{\psi_1} \frac{(\omega_1)^{N_1}}{N_1!} \right) \left(\prod_{q_2=1}^{\psi_2} \frac{(\omega_2)^{N_2}}{N_2!} \right) = N! \left(\frac{(\omega_1)^{N_1}}{N_1!} \right)^{\psi_1} \left(\frac{(\omega_2)^{N_2}}{N_2!} \right)^{\psi_2}. \tag{92}$$

Similarly, if there are J groups with similar number of configurations and number of chains in each group

$$\Omega^t = N! \prod_{j=1}^{J} \left(\frac{(\omega_j)^{N_j}}{N_j!} \right)^{\psi_j}, \tag{93}$$

where ψ_j is the number of end-to-end vectors in the j-th group and

$$\sum_j \psi_j N_j = N. \tag{94}$$

The number of possible configurations of a polymer chain is calculated as

$$\omega_j = \frac{n_j!}{\Pi_i \left(n_{ij}!\right)}, \tag{95}$$

where n_j is the number of dipolar monomers in a chain which is in the j-th group of chains and n_{ij} is the number of monomers aligned along $\hat{\boldsymbol{\xi}}_i$ in a chain which is in the j-th group. Consequently, the total entropy of the polymer

$$\begin{aligned} S^t &= k \ln \left(\Omega^t \right) \\ &= k \left(N \ln (N) - N + \sum_j \psi_j \left(N_j \left(n_j \ln (n_j) - n_j - \sum_i n_{ij} \ln (n_{ij}) + \sum_i n_{ij} \right) - N_j \ln (N_j) + N_j \right) \right) \\ &= k \left(N \ln (N) + \sum_j \psi_j N_j \left(n_j \ln (n_j) - \sum_i n_{ij} \ln (n_{ij}) - \ln (N_j) \right) \right), \end{aligned} \tag{96}$$

by employing the Stirling approximation. The polymer network is subjected to the constraint mentioned in Eq. (94). As was previously specified, each chain is subjected to three constraints:

$$\sum_i n_{ij} = n_j, \tag{97}$$

$$\sum_i l n_{ij} \hat{\boldsymbol{\xi}}_i = \mathbf{r}_j, \tag{98}$$

and the end-to-end vector of the monomers chain is $\mathbf{r}_j = r_j \, \hat{\mathbf{r}}_j$, and

$$\sum_i n_{ij} h_i = H_j^C, \tag{99}$$

where H_j^C is the electrical-enthalpy of the chain and h_i is the enthalpy of a monomer aligned along $\hat{\boldsymbol{\xi}}_i$.

We assume that the most probable configuration is the one that the polymer occupies, and thus we are interested in maximizing the entropy under the given constraints,

$$S^t = k\,\ln\left(\Omega_t\right) + k\,\sum_j \psi_j N_j \left(\alpha_j \left(\sum_i n_{ij} - n_j\right) + \boldsymbol{\tau}_j \cdot \left(\sum_i n_{ij}\hat{\boldsymbol{\xi}}_i - \frac{\mathbf{r}_j}{l}\right) + \gamma_j \left(\sum_i n_{ij} h_i - H_j^C\right)\right) + k\,\eta\left(\sum_j \psi_j N_j - N\right), \tag{100}$$

where α_j, $\boldsymbol{\tau}_j$, γ_j and η are Lagrange multipliers.

In order to account for the maximal number of configurations we impose that

$$\frac{\partial S^t}{\partial n_{ij}} = k\,\left(-\psi_j N_j \ln\left(n_{ij}\right) + \psi_j N_j \left(\alpha_j + \boldsymbol{\tau}_j \cdot \hat{\boldsymbol{\xi}}_i + \gamma_j h_i\right)\right) = 0, \tag{101}$$

from which

$$n_{ij} = \exp\left(\frac{\psi_j N_j \left(\alpha_j + \boldsymbol{\tau}_j \cdot \hat{\boldsymbol{\xi}}_i + \gamma_j h_i\right)}{\psi_j N_j}\right) = \exp\left(\alpha_j + \boldsymbol{\tau}_j \cdot \hat{\boldsymbol{\xi}}_i + \gamma_j h_i\right). \tag{102}$$

By substituting Eq. (101) in Eq. (100), the maximum entropy of the polymer is

$$S^t = k\,N\ln\left(N\right) + k\,\sum_j \psi_j \left(N_j\left(n_j \ln\left(n_j\right)\right) - N_j \ln\left(N_j\right)\right) - \sum_j \psi_j N_j \left(\alpha_j n_j + \boldsymbol{\tau}_j \cdot \frac{\mathbf{r}_j}{l} + \gamma_j H_j^C\right) + k\,\eta\left(\sum_j \psi_j N_j - N\right). \tag{103}$$

Following the works of Kuhn and Grün [1942] and Treloar [1975], we too assume the polymer chains do not interact with one another. Therefore, the total enthalpy is $H_t = \sum_j \psi_j N_j H_j^C$. Differentiating the first law of thermodynamics, Eq. (8), with respect to the enthalpy of the j'th we have that

$$\frac{\partial H^t}{\partial H_j^C} = T\frac{\partial S^t}{\partial H_j^C}, \tag{104}$$

and by using Eq. (103) we derive the relation

$$\gamma_j = -\frac{1}{k\,T}. \tag{105}$$

By taking into consideration the constraint in Eq. (97) and the relations we received

in Eq. (102) and (105) we obtain that

$$\sum_i n_{ij} = \int_0^{\Gamma_0} \exp\left(\alpha_j + \boldsymbol{\tau}_j \cdot \hat{\boldsymbol{\xi}}_i - \frac{h_i}{k\,T}\right) \mathrm{d}\Gamma = n_j. \tag{106}$$

From here we can determine the PDF that a monomer in the j-th chain is in the direction of $\hat{\boldsymbol{\xi}}_i$ and has an electrical-enthalpy h_i. This is

$$p_{ij}\left(\hat{\boldsymbol{\xi}}_i, h_i\right) = \frac{n_{ij}}{n_j} = \frac{1}{Z_j} \exp\left(\boldsymbol{\tau}_j \cdot \hat{\boldsymbol{\xi}}_i - \frac{h_i}{k\,T}\right), \tag{107}$$

where

$$Z_j = \int_0^{\Gamma_0} \exp\left(\boldsymbol{\tau}_j \cdot \hat{\boldsymbol{\xi}}_i - \frac{h_i}{k\,T}\right) \mathrm{d}\Gamma, \tag{108}$$

is the partition function and the Lagrange multipliers $\boldsymbol{\tau}_j$ are computed from the implicit equations that follow from the constraints in Eq. (98),

$$\int_0^{\Gamma_0} \hat{\boldsymbol{\xi}}_i\, p_{ij}\, \mathrm{d}\Gamma = \frac{\mathbf{r}_j}{n_j\, l}. \tag{109}$$

The enthalpy of the chain,

$$\int_0^{\Gamma_0} h_i\, p_{ij}\, \mathrm{d}\Gamma = H_j^C, \tag{110}$$

is computed from constraint Eq. (99).

In order to consider the network with largest number of chain configurations we impose that

$$\begin{aligned}
\frac{\partial S^t}{\partial N_j} &= \psi_j \left(n_j \ln\left(n_j\right) - \sum_i n_{ij} \ln\left(n_{ij}\right) - \ln\left(N_j\right)\right) + \psi_j \alpha_j \left(\sum_i n_{ij} - n_j\right) + \psi_j \boldsymbol{\tau}_j \cdot \left(\sum_i n_{ij} \hat{\boldsymbol{\xi}}_i - \frac{\mathbf{r}_j}{l}\right) \\
&\quad + \psi_j \gamma_j \left(\sum_i n_{ij} h_i - H_j^C\right) + \eta \psi_j \\
&= \psi_j \left(n_j \ln\left(n_j\right) - \sum_i n_{ij} \ln\left(n_{ij}\right) - \ln\left(N_j\right) + \eta\right) = 0,
\end{aligned} \tag{111}$$

from which

$$N_j = \exp\left(n_j \ln\left(n_j\right) - \sum_i n_{ij} \ln\left(n_{ij}\right) + \eta\right) = \frac{\exp\left(\eta\right)\, n_j^{n_j}}{\prod_i n_{ij}^{n_{ij}}}. \tag{112}$$

Next, from constraint Eq. (94) we obtained that

$$\sum_j \psi_j N_j = \sum_j \psi_j \frac{\exp(\eta)\ n_j^{n_j}}{\prod_i n_{ij}^{n_{ij}}} = N. \tag{113}$$

This enables us to determine the Lagrange multiplier

$$\eta = \ln\left(\frac{N}{\sum_j \left(\frac{\psi_j n_j^{n_j}}{\prod_i n_{ij}^{n_{ij}}}\right)}\right). \tag{114}$$

Furthermore, the PDF that a chain is in the j-th inclination is

$$p_j = \frac{N_j}{N} = \frac{\prod_i n_{ij}^{-n_{ij}}}{\sum_k \psi_k \prod_i n_{ik}^{-n_{ik}}} = \frac{\prod_i (n_j p_{ij})^{-n_j p_{ij}}}{\sum_k \psi_k \prod_i (n_k p_{ik})^{-n_k p_{ik}}}, \tag{115}$$

and the fraction of all the chains with a specific inclination to the electric field can be estimated as

$$\upsilon_j = \psi_j p_j, \tag{116}$$

such that $\sum_j \upsilon_j = 1$.

Next, we make use of Eq. (115) in Eq. (103) to determine the entropy of the entire network

$$\begin{aligned} S^t = k \left(N \ln(N) + \sum_j \psi_j N_j \left(n_j \ln(n_j) - \sum_i n_{ij} \ln(n_{ij}) - \ln\left(N \frac{\prod_i n_{ij}^{-n_{ij}}}{\sum_k \psi_k \prod_i n_{ik}^{-n_{ik}}}\right)\right)\right) \\ = k\, N \ln(N) + k \sum_j \psi_j N_j \left(n_j \ln(n_j) - \sum_i n_{ij} \ln(n_{ij}) - \ln(N)\right) \\ + k \sum_j \psi_j N_j \left(\sum_i n_{ij} \ln(n_{ij}) + \ln\left(\sum_k \psi_k \prod_i n_{ik}^{-n_{ik}}\right)\right) \\ = k \left(\sum_j \psi_j N_j \left(n_j \ln(n_j) + \ln\left(\sum_k \psi_k \prod_i n_{ik}^{-n_{ik}}\right)\right)\right). \end{aligned} \tag{117}$$

Assuming that the number of dipolar monomers in each chain is fixed, we neglect the first term in the last of Eq. (117) to conclude that

$$S^t \propto N \ln\left(\sum_k \psi_k \prod_i n_{ik}^{-n_{ik}}\right). \tag{118}$$

By following the same steps for the case of the entropy of a chain presented in Eq. (22), it can be concluded that

$$S_j^C \propto \ln\left(\prod_i n_{ij}^{-n_{ij}}\right). \tag{119}$$

We can observe the similarities between both assessments of the maximum entropy. In Eq. (119) the entropy of a chain is a function of the end-to-end, r_j, and does not depend on the inclination, $\hat{\mathbf{r}}$.

We note that in the case of exitation by an electric field the number of end-to-end vectors in the j-th group are dependent on the groups inclinations to the direction of the electric field, and so

$$\psi_j = 2\pi r_j^2 \sin\left(\Theta_j\right). \tag{120}$$

3.4.1 Deriving the properties of the polymer

In order to assess our methodology, we wish to evaluate the properties of the new anisotropic polymer and to compare them to those of the isotropic polymer. Besides the electro-mechanical coupling, which is our main interest, the response of the polymer to purely mechanical loading and electrostatic exitation should be examined too. The mechanical properties of the polymer relate to the mechanical stress in the polymer under purely mechanical loading described by the deformation gradient tensor $\boldsymbol{F}$. The electrical properties of the polymer, such as the electric displacement and the susceptibility, relate to the polarization in the polymer under electrostatic exitation.

(Note: referenced mechanical stress)

The general mechanical stress presented by Cohen et al. [2016] which results from Eq. (16) is

$$\boldsymbol{\sigma}^m = \frac{1}{J\,\mathrm{dV}_0}\sum_i \left(n \left(\int_0^{\Gamma_0} \frac{\partial h}{\partial \boldsymbol{F}}\, p\,\mathrm{d}\Gamma \right)_i + \frac{k\,T\,\boldsymbol{\tau}_i}{l}\frac{\partial \mathbf{r}_i}{\partial \boldsymbol{F}} \right) \boldsymbol{F}^{\mathrm{T}}. \tag{121}$$

The mechanical stress takes into account the change in the electrical energy of a the monomers due to the mechanical deformation and for the mechanical loadings that deforms the chains end-to-end vectors. Considering the assumption made by Cohen et al. [2016] that the monomer is rigid compared to the polymer chain, the electrical enthalpy of the monomer does not depend on the deformation gradient. Furthermore, by assuming an incompressible material, Eq. (121) can be simplified to

$$\boldsymbol{\sigma}^m = \frac{1}{\mathrm{dV}_0}\sum_i \left(\frac{k\,T\,\boldsymbol{\tau}_i}{l}\frac{\partial \mathbf{r}_i}{\partial \boldsymbol{F}} \right) \boldsymbol{F}^{\mathrm{T}}. \tag{122}$$

(Note: simplified mechanical stress, suitable for an anisotropic case)

In order to evaluate the mechanical stress in the polymer, the average stress of each chain group is calculated first. As mentioned, in the case of exitation by an electric field, the chains groups are determined by their inclinations to the direction of the electric field.

Thus, the stresses of chains with the same inclination, Θ_k, are averaged over $0 \leq \Phi_q < 2\pi$

$$\boldsymbol{\sigma}_k^m = \frac{\sum_q^Q \left(\frac{k\,T\,\boldsymbol{\tau}_{kq}}{l} \frac{\partial \mathbf{r}_{kq}}{\partial \boldsymbol{F}} \right) \boldsymbol{F}^{\mathrm{T}}}{Q}, \tag{123}$$

where $\hat{\mathbf{r}}_{kq} = \cos\Theta_k \hat{\mathbf{E}} + \sin\Theta_k \left(\cos\Phi_q \hat{\mathbf{Y}} + \sin\Phi_q \hat{\mathbf{Z}} \right)$, as $q = 1, 2, ..., Q$. $\frac{\partial \mathbf{r}_{kq}}{\partial \boldsymbol{F}}$ is detailed in appendix B.

Next, the relative influence of each of the chains groups is considered. This is performed by taking into account the fraction of the chains in a specific group, as shown in Eq. (116). Thus, Eq. (122) can be rewritten as

$$\boldsymbol{\sigma}^m = N \sum_k \upsilon_k \boldsymbol{\sigma}_k^m, \tag{124}$$

where the averaged stress of a chain is multiplied by the number of chains in a unit volume, N.

(Note: referenced polarization)

The polarization

$$\mathbf{P} = -\frac{1}{J\,\mathrm{dV}_0} \sum_i \left(n \left(\int_0^{\Gamma_0} \frac{\partial h}{\partial \mathbf{E}}\, p\, \mathrm{d}\Gamma \right)_i + \frac{k\,T\,\boldsymbol{\tau}_i}{l} \frac{\partial \mathbf{r}_i}{\partial \mathbf{E}} \right), \tag{125}$$

was presented by Cohen et al. [2016]. This relations stems from Eq. (17). The polarization equation, Eq. (125), considers the variation of the electrical enthalpies of the monomers as a result of the excitation of the electric field and the reorientation of the chains as a response to the electrical excitation. From the assumption that the chains undergo affine deformation, it follows that the electric field does not directly affect the distribution of the chains. Thus, by assuming an incompressible material, Eq. (125) can be simplified to

$$\mathbf{P} = -\frac{n}{\mathrm{dV}_0} \sum_i \left(\int_0^{\Gamma_0} \frac{\partial h}{\partial \mathbf{E}}\, p\, \mathrm{d}\Gamma \right)_i. \tag{126}$$

(Note: simplified polarization, suitable for an anisotropic case + susceptibility)

The polarization of the polymer is calculated by executing the same steps that were described for the mechanical stress. As $\frac{\partial h}{\partial \mathbf{E}} = -\mathbf{m}$, the polarizations of chains with the same inclination, Θ_k, are averaged over $0 \leq \Phi_q < 2\pi$

$$\mathbf{P}_k = \frac{n \sum_q^Q \left(\int_0^{\Gamma_0} \mathbf{m}\, p\, \mathrm{d}\Gamma \right)_{kq}}{Q}, \tag{127}$$

where $q = 1, 2, ..., Q$.

Thus, as the relative influence of each of the chains groups is considered through the fraction of the chains in a specific group,

$$\mathbf{P} = N \sum_k \upsilon_k \mathbf{P}_k, \tag{128}$$

where the averaged polarization of a chain is multiplied by the number of chains in a unit volume, N. After the calculation of the polarization, the electric displacement can be calculated according to Eq. (3) and the susceptibility can be calculated as

$$\chi = \frac{\mathbf{P} \cdot \mathbf{E}}{\epsilon_0 E^2}. \tag{129}$$

4 Application to electrostatically biased network

(Note: Opening sentence + Isotropic example - first step of the numerical analysis - evaluating the Lagrange multiplier tau**)**

As we aspire to modify the properties of DEs in order to affect their electromechanical coupling, we propose to perform the polymerization process of a polymer while in the presence of an electric field. Such a process will result in a relative order of the networks of polymer chains as the chains and the dipolar monomers can react to the electric field while the chains are forming and "floating" in the solution state. The mentioned electric field will be removed at the end of the hardening of the network which is a result of the cross-linking of the chains. We note that the responses of the chains and monomers are restricted by the constraints in Eq. (94), Eq. (97), Eq. (98) and Eq. (99), as is detailed in section 3.4.

For the sake of examining the influence of our proposed polymerization process (i.e. creating a “biased” polymer), we follow the analytical analysis detailed in section 3. This examination will be executed while comparing our results for the biased polymer to those of an unbiased polymer (i.e. an isotropic polymer) and to the IED model (presented in section 2.3), all in order to evaluate the influence of performing the suggested process on the structure and properties of the polymer.

4.1 Chains distribution

The initial step of the analysis is to evaluate the most probable configurations of the polymer chains in the isotropic and biased polymers. At first we apply our calculations to the case of no electric field, for an isotropic chain network. The initial step of the calculation is to evaluate the value of the Lagrange multiplier $\boldsymbol{\tau}$ with the application of the Newton-Raphson method on Eq. (36). The first guess, $\boldsymbol{\tau}_0$, is obtained by analytically estimating the Lagrange multiplier as a function of $\mathbf{r}$ in a case where the electric field approaches zero,

$$\boldsymbol{\tau}_0 = \frac{3\mathbf{r}}{n\,l}, \tag{130}$$

which is accurate in this specific case, as is detailed in appendix C.

(Note: chains length - isotropic distribution**)**

As a result of the maximum-entropy assumption and the fact that, in this case, there is no electric actuation or any other external influence we can assume that there is an isotropic distribution of chains and so we can assess the end-to-end length of a chain in a single direction and relate it to all directions. Thus, in order to evaluate the most probable end-to-end chain length, the number of configuration of a chain with a specific $\mathbf{r}$ is calculated and then multiplied by the surface area of a sphere with the same r,

which represents the chains groups in the isotropic case, as is discussed in section 3.2.3 and shown in Eq. (81). The entropy of each case is calculated by using the results from Eq. (81) in Eq. (22). An example is presented in Fig. 6, which presents the entropy as a function of the normalized radius, $\frac{r}{nl}$, for $n = 50$ and $n = 100$ as $l = 100\,\mu$m. The initial susceptibility used in the presented exampels is $\chi_0 = 37$, about ten times the electric susceptibility of the commercially available VHB 4910. The analyses are performed for the case of uniaxial dipoles. The difference between the curves in Fig. 6 can be attributed to Eq. (21), Eq. (22) and Eq. (81). Accordingly, as the number of monomers in a chain increases so does the entropy of the chain.

(Note: defining calculation parameters - material properties and calculations boundaries)

We assume that the shear modulus of the polymer in its initial unloaded configuration is $\mu = 10^5$ Pa. The value of N, the number of chains in a unit volume, was deduced from the relation $\mu = N\,k\,T$ [Treloar, 1943, Flory and Rehner, 1943]. The normalized radii that correspond to the maximum points of the two curves in Fig. 6 are $\left(\frac{r}{nl}\right)_{n=50} \cong 0.1$ and $\left(\frac{r}{nl}\right)_{n=100} \cong 0.075$ which are compatible to the analytical predictions given in section 3.2.3, of $\left(\frac{r}{nl}\right)_{n=50} = 0.115$ and $\left(\frac{r}{nl}\right)_{n=100} = 0.082$, presented by the dashed columns in Fig. 6. The differences between the numerical and analytical results for the most probable end-to-end chain length can be associated with the density of discretization of 0.025 for $0 \leq \frac{r}{nl} \leq 1$. Furthermore, it can be seen that the results of the current approach are different from the results of the random walk statistics of $\left(\frac{r}{nl}\right)_{n=50} = 0.141$ and $\left(\frac{r}{nl}\right)_{n=100} = 0.1$, presented by the dot-dashed columns in Fig. 6. The values of the entropy that are smaller then zero are irrational and are truncated as they represent numbers of configurations that are not compatible with the previously made assumption for Stirling's approximation between Eq. (21) and Eq. (22).

(Note: the main idea - parameters value and initial calculations)

Next, for the purpose of evaluating the influences of electrical exitation on the polymer structure during a polymerization process, different parameters were investigated as the electric field magnitude ranged from $0\,\frac{\mathrm{MV}}{\mathrm{m}}$ to $150\,\frac{\mathrm{MV}}{\mathrm{m}}$. The presented results are based on numerical calculation where the number of monomers in a single chain, the length between the two contact points of a monomer with its neighbors and the number of chains in a unit volume are the same as the ones assumed for the case of no electric field.

In order to demonstrate the influence of electric fields with different magnitudes on chains at various inclinations to the direction of the field, results for chains with $\Theta = \frac{\pi}{1000}$, $\Theta = \frac{\pi}{4}$ and $\Theta = \frac{\pi}{2}$ are presented in Fig. 7, Fig. 8 and Fig. 9. The natural logarithm of the maximum number of configurations for each chain as a function of the electric field can be seen in Fig. 7. The end-to-end length with the maximum number of configurations of each chain as a function of the electric field can be seen in Fig. 8. The Lagrange multiplier $\boldsymbol{\tau}$, which can be portrayed as the chain's mechanical constraint, that relates

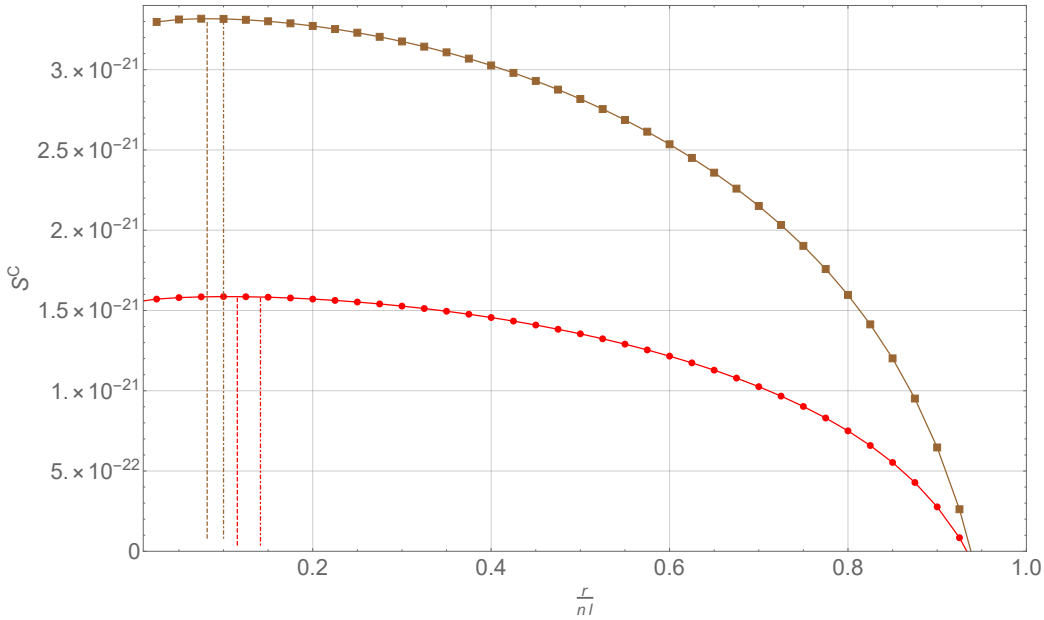

Figure 6: The entropy of a polymer chain with uniaxial dipoles as a function of the normalized radius as $0 \leq \frac{r}{nl} \leq 1$ and $l = 100\,\mu$m. The red continuous curve with circular markers corresponds to $n = 50$ and the brown curve with squares to $n = 100$. The dashed columns corresponds to the normalized radii in accordance with the results in section 3.2.3, $\frac{r}{nl} = \sqrt{\frac{2}{3}}\frac{1}{\sqrt{n}}$, and the dot-dashed columns to the results from random walk statistics, $\frac{r}{nl} = \frac{1}{\sqrt{n}}$.

to the end-to-end length with the maximum number of configurations was examined as a function of the electric field magnitude, as can be seen in Fig. 9.

We note from Fig. 7, Fig. 8 and Fig. 9, that the magnitude range of electric field that is smaller than $50\,\frac{\text{MV}}{\text{m}}$ has shown very small differences in results from the case of $E = 0\,\frac{\text{MV}}{\text{m}}$. This is particularly evident in Fig. 8, where the change in the end-to-end length of the different chains is hardly visible below $50\,\frac{\text{MV}}{\text{m}}$. In Fig. 7, we can observe the similarities in the curves for the natural logarithm of the maximum number of configurations for chains at different inclinations, which all decrease as the magnitude of the electric field is enhanced. The differences between the curves can be associated to the number of end-to-end vectors in each inclination to the direction of the electric field, seen in Eq. (120). By observing Fig. 8, it can be seen that the end-to-end length of chains at all inclinations increase as the magnitude of the electric field is enhanced. Though, as the magnitude is enhanced, the differences in the end-to-end length become more prominent, as chains in greater inclinetions are longer. We find that this is counterintuitive as we would expect chains with greater inclinations to the direction of the electric field to be shorter as the monomers aspire to reorient in the direction of the electric field. From Fig. 9 we can observe the differences in the chains mechanical constraint. As the magnitude of the electric field is enhanced its value decreases for chains parallel to the direction of the electric field and

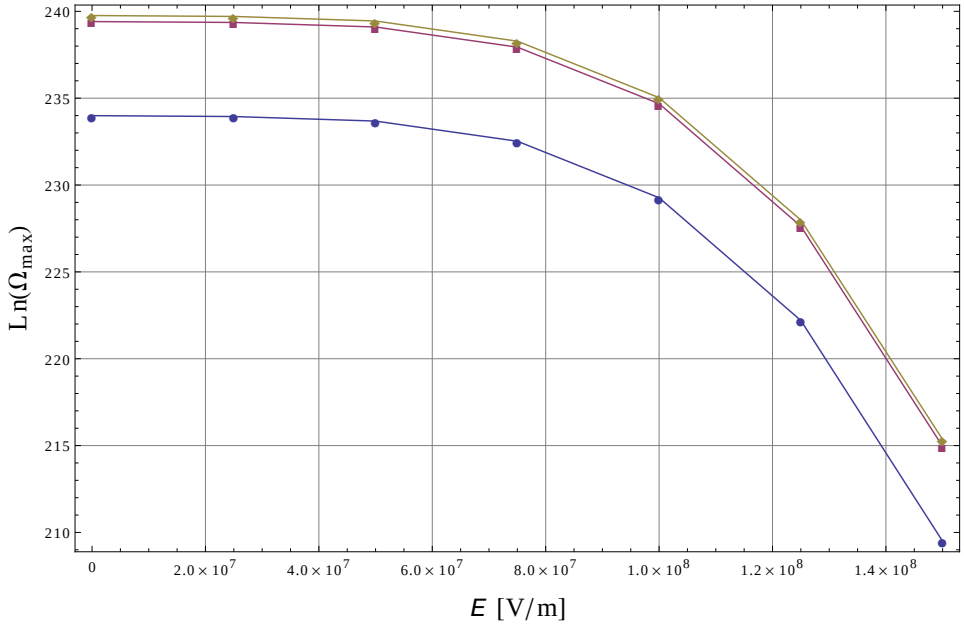

Figure 7: The natural logarithm for the maximum number of configurations as a function of the electric field magnitude for chains with uniaxial dipoles at different inclinations. The blue curve with circular markers corresponds to $\Theta = \frac{\pi}{1000}$, the red curve with squares to $\Theta = \frac{\pi}{4}$ and the yellow curve with diamonds to $\Theta = \frac{\pi}{2}$.

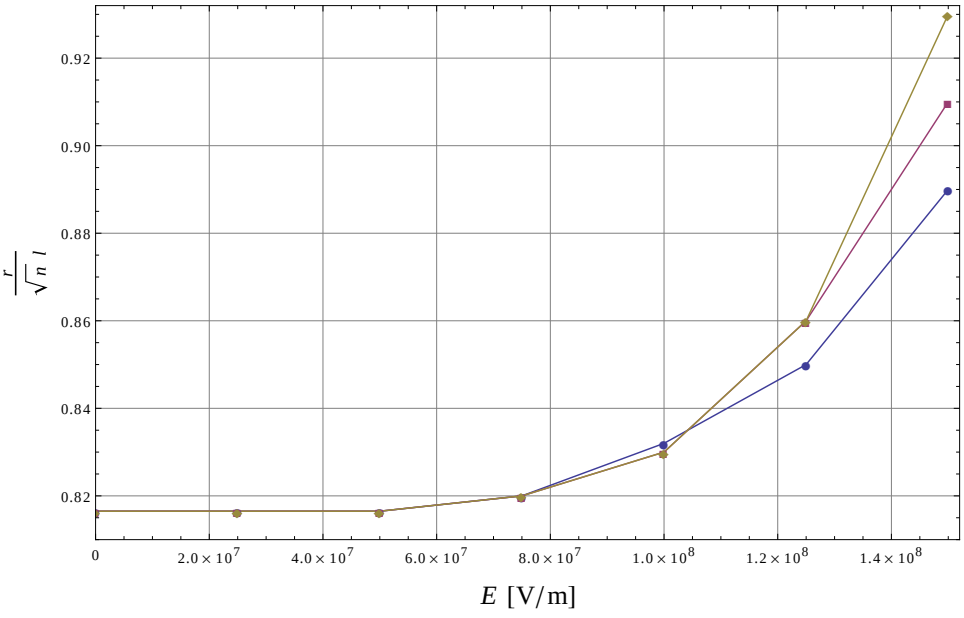

Figure 8: The most probable end-to-end length as a function of the electric field magnitude for chains with uniaxial dipoles at different inclinations. The blue curve with circular markers corresponds to $\Theta = \frac{\pi}{1000}$, the red curve with squares to $\Theta = \frac{\pi}{4}$ and the yellow curve with diamonds to $\Theta = \frac{\pi}{2}$.

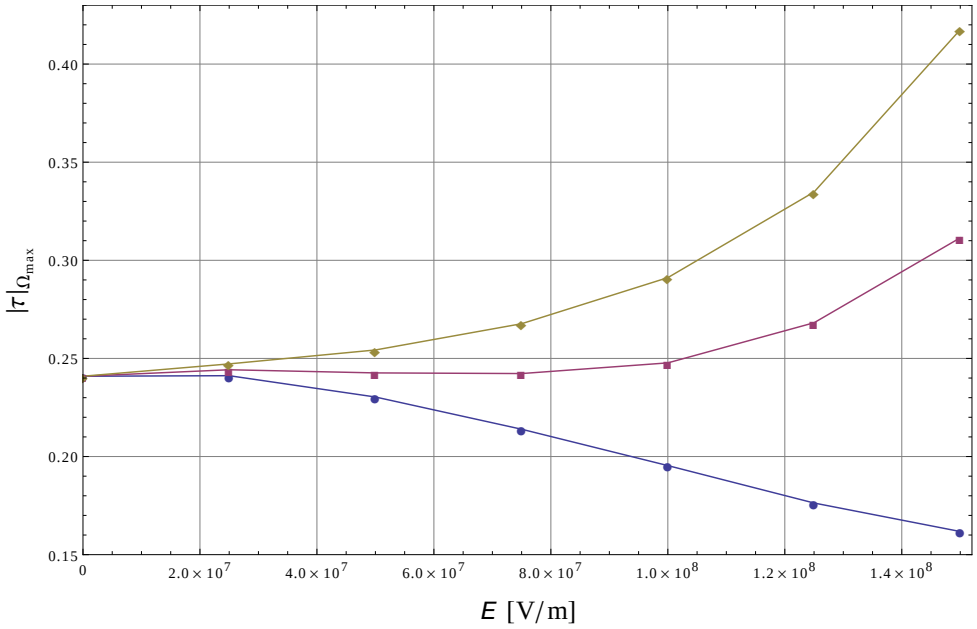

Figure 9: The size of the Lagrange multiplier $\boldsymbol{\tau}$, associated with the most probable radius as a function of the electric field magnitude for chains with uniaxial dipoles at different inclinations. The blue curve with circular markers corresponds to $\Theta = \frac{\pi}{1000}$, the red curve with squares to $\Theta = \frac{\pi}{4}$ and the yellow curve with diamonds to $\Theta = \frac{\pi}{2}$.

relatively increases for chains with greater inclinations. This can be attributed to the fact that as the polymer is in a solution state during the polymerization, it is "harder" to hold chains at larger inclinations as the monomers react to the electric exitation and aspire to rotate towards its direction.

4.2 Monomers orientation

(Note: monomer distribution - chains)

Once the calculations of the end-to-end lengths for chains at each of the mentioned inclination to the direction of the electric field, i.e. determining $\mathbf{r}_j^0 = r^0(\Theta_j, \mathbf{E})\,\hat{\mathbf{r}}(\Theta_j)$, the monomers orientation can be calculated as detailed in section 3.3.1. Fig. 10a, b and c present the monomers distribution of chains with different inclinations $\Theta = \frac{\pi}{1000}$, $\Theta = \frac{\pi}{4}$ and $\Theta = \frac{\pi}{2}$, respectively, while the magnitude of the electric field is $E = 150\,\frac{\mathrm{MV}}{\mathrm{m}}$. In these three dimensional plots, the length of the radius vector to each point represents the number of monomers aligned with this vector. As can also be seen, the monomers distributions are compatible when comparing between the different inclinations. This means that the monomers in the different chains aspire to orient similarly. This compatibility is very interesting, as the chains have different inclinations and different end-to-end lengths.

(Note: amorphous monomer distribution)

As the monomers orientation for each of the mentioned chains was obtained and their

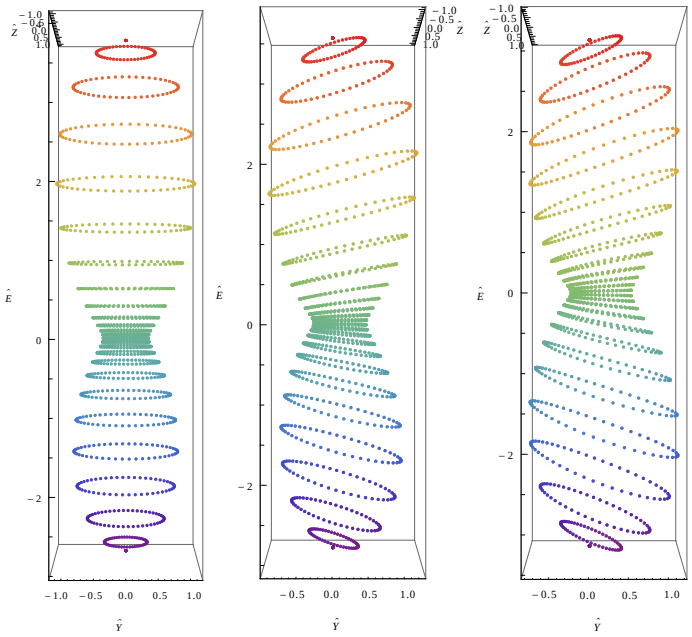

(a) (b) (c)

Figure 10: The monomer distribution for a polymer chain of uniaxial dipoles. The magnitude of the electric field during the polymerization process is $E = 150\,\frac{\mathrm{MV}}{\mathrm{m}}$. (a) Corresponds to the chain with the inclination $\Theta = \frac{\pi}{1000}$ and end-to-end length $r = 0.89\sqrt{n}\,l$. (b) Corresponds to $\Theta = \frac{\pi}{4}$ and $r = 0.91\sqrt{n}\,l$. (c) Corresponds to $\Theta = \frac{\pi}{2}$ and $r = 0.93\sqrt{n}\,l$.

likeness was recognized, the monomers distribution in an amorphous case is examined. Fig. 11 presents the results of the numerical calculations for amorphous monomers distribution in the case of a uniaxial dipole according to Eq. (42). Unlike Fig. 10a, b and c, Fig. 11 presents a symmetric distribution of the monomers, as in this case the monomers are free to reorient separately and are not constrained as a part of a chain. The result of the analytical analysis for the PDF in the amorphous case [Cohen et al., 2016], presented in Eq. (44) can also be seen in Fig. 11 as they are identical to the numerical results.

4.3 The free state

(Note: finding the natural state - chains distribution, weights and lambda0 deformation)

After analyzing the micro-scale and understanding the monomer distribution as a result of the mentioned polymerization process, the macro-scale is examined. Hence, as we wish to analyze the macroscopic response of the polymer to different excitations, as is detailed in section 3.4, the relative influence of each of the chains groups in the different inclinations needs to be assessed. For the sake of such evaluation Eq. (116) and Eq. (120) are used to calculate the fraction of chains with the j-th inclination to the electric field. A comparison of the number of chains in the different inclinations to the direction of the

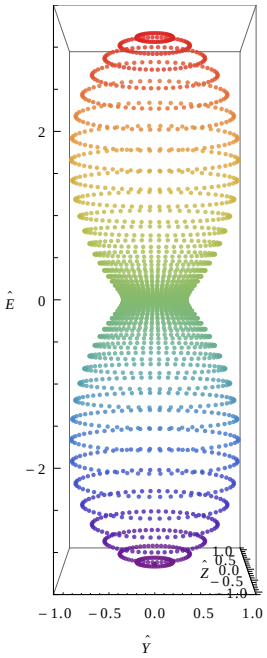

Figure 11: The amorphous monomer distribution of a uniaxial dipole as $E = 150\,\frac{\mathrm{MV}}{\mathrm{m}}$. According to the numerical analysis as $\boldsymbol{\tau} = 0$ and identical to the results of the analytical analysis that was presented by Cohen et al. [2016].

electric field between the isotropic polymer and the biased polymer is presented in Fig. 12. A comparison between the fractions of chains in each inclination of both cases is presented in Fig. 13. The relations between the results in Fig. 12 and Fig. 13 are credited to ψ_j, which is the number of end-to-end vectors in the j-th group, presented in Eq. (120).

As can be observed from Fig. 12, the presence of an electric field in the polymerization process affects the distribution of the chains, as the chains aspire to align in the direction of the electric field. Though, as a result of Eq. (120) and as can be observed in Fig. 13, the most influential inclination of the polymer as a result of the proposed process is $\Theta \cong \frac{\pi}{4}$.

The density of discretization for the inclinations to the direction of the electric field is taken as $\Delta\Theta = \frac{\pi}{16}$, as denser discretizations did not produce any meaningful differences in the results. As we refer to the different groups of chains discreetly in accordance with their inclinations to the direction of the electric field, we attribute each group chains with one end at the origin and the other end located within a small volume $\mathrm{d}V = r^2 \mathrm{d}r\mathrm{d}\phi\mathrm{d}\theta$. Furthermore, we note that as the coupling in DEs is characterized by a quadratic dependence on the applied electric potential [Toupin, 1956], the different responses of DEs can be deduced from analyzing $0 \leq \Theta \leq \frac{\pi}{2}$. Accordingly, the groups that relates to inclinations $\Theta = 0$ and $\Theta = \frac{\pi}{2}$, which are the boundaries of the analyzed range, are attributed to small volumes with $\Delta\Theta = \frac{\pi}{32}$. This is performed so as not to exceed the limits set for the tested angular range.

Fig. 14 presents the analysis of the deformation in the direction of the electric field,

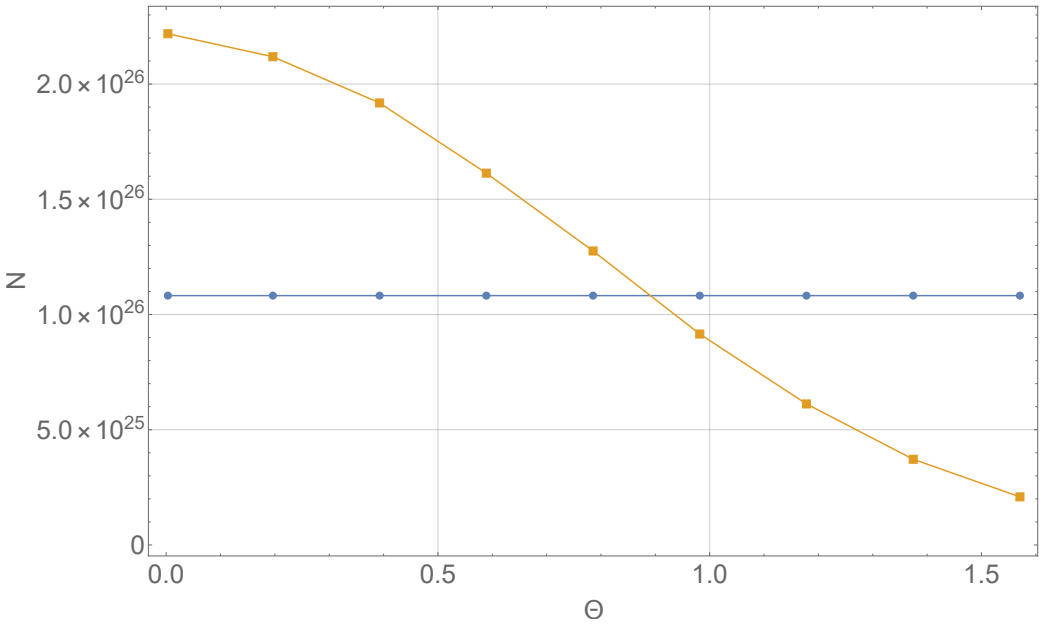

Figure 12: The number of chains along each inclination as a function of the inclination relative to the direction of the electric field, $N(\Theta, \Phi = 0)$. The blue curve with circular markers corresponds to the isotropic polymer and the yellow curve with squares corresponds to the biased polymer.

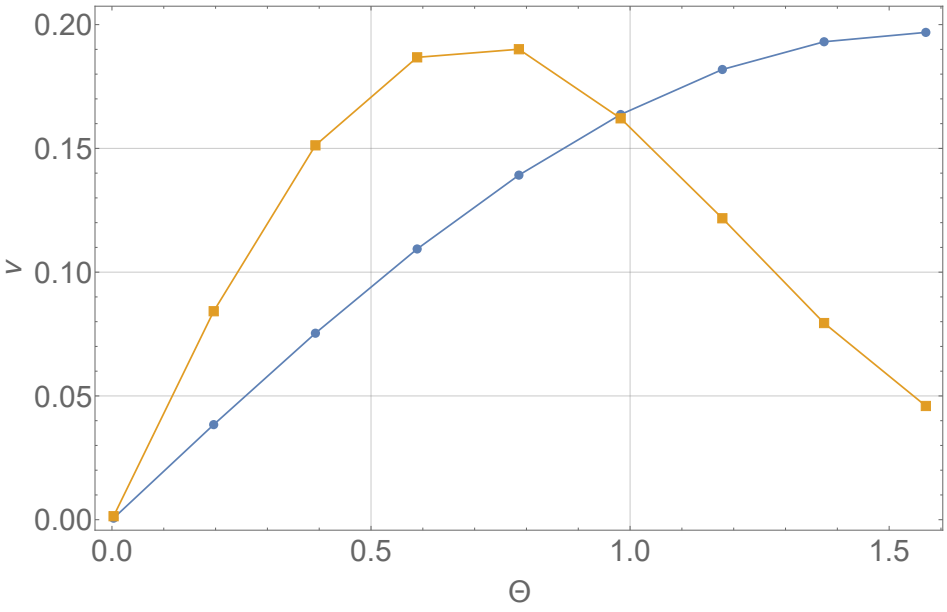

Figure 13: The fractions of chains along each inclination as a function of the inclination to the direction of the electric field, $\nu(\Theta)$. The blue curve with circular markers corresponds to the isotropic polymer and the yellow curve with squares corresponds to the biased polymer.

λ_0, of a polymer that was induced with the chosen electric field magnitude during the polymerization process, as the electric field is removed at the end of the process. The chains are unable to change their lengths to the length of the chains in the isotropic polymer as they are cross-linked and cannot rearrange separately. Thus, each chain is affected by the same deformation gradient. The corresponding deformation gradient, while assuming incompressibility, is

$$\boldsymbol{F}^0(\lambda_0) = \lambda_0 \hat{\mathbf{E}} \otimes \hat{\mathbf{E}} + \frac{1}{\sqrt{\lambda_0}} \left(\boldsymbol{I} - \hat{\mathbf{E}} \otimes \hat{\mathbf{E}} \right) = \begin{pmatrix} \lambda_0 & 0 & 0 \\ 0 & 1/\sqrt{\lambda_0} & 0 \\ 0 & 0 & 1/\sqrt{\lambda_0} \end{pmatrix}. \tag{131}$$

In order to assess the stress free configuration of an incompressible body such as the biased polymer, different deformation gradients were examined. The suitable one is depicted by the state where $\boldsymbol{\sigma}_{\mathrm{EE}} = \boldsymbol{\sigma}_{\mathrm{YY}} = \boldsymbol{\sigma}_{\mathrm{ZZ}} = \frac{\mathrm{Tr}(\boldsymbol{\sigma})}{3}$ as the deviatoric stress is zero in accordance with Eq. (19). As seen in Fig. 14, λ_0 is achieved from calculating $\boldsymbol{\sigma}_{\mathrm{EE}} - \boldsymbol{\sigma}_{\mathrm{YY}} = \boldsymbol{\sigma}_{\mathrm{Diff}}$ and determining the correct value from $\boldsymbol{\sigma}_{\mathrm{Diff}}(\lambda_0) = 0$. In this case it is received for λ_0=0.795, which means that the deformation gradient tensor that is compatible with the deformation after the removal of the electric field is

$$\boldsymbol{F}^0_{E=150\,\frac{\mathrm{MV}}{\mathrm{m}}} = \begin{pmatrix} 0.795 & 0 & 0 \\ 0 & 1.121 & 0 \\ 0 & 0 & 1.121 \end{pmatrix}. \tag{132}$$

This is counterintuitive when considering that in this case chains in greater inclinations will get longer. Though, when considering the orientation of the monomers, it is reasonable to assume that some will rearrange in grater inclination to the electric field as it is removed. Thus, the polymer will perform a planar expansion. The chains end-to-end lengths and inclinations in the relaxed state, which from now on will be the starting point for each of the examined chains in the biased polymer, can be deduced from $\mathbf{r}_j = \boldsymbol{F}^0 \mathbf{r}^0_j$. We also note that the same calculations for the isotropic case yielded $\lambda^{\mathrm{Iso}}_0 = 1$, as was expected.

4.4 The materials properties

(Note: mechanical and electrostatic properties - new polymer + comparison)

As the chains orientations were established for the mentioned example, the properties of the biased polymer can be examined and compared to the case of an isotropic polymer, as detailed in section 3.4.1. The polymer's mechanical properties can be assessed by evaluating the mechanical stresses as a function of the deformation ratio, λ, according to Eq. (124). The calculationes of the mechanical stresses were performed by taking into

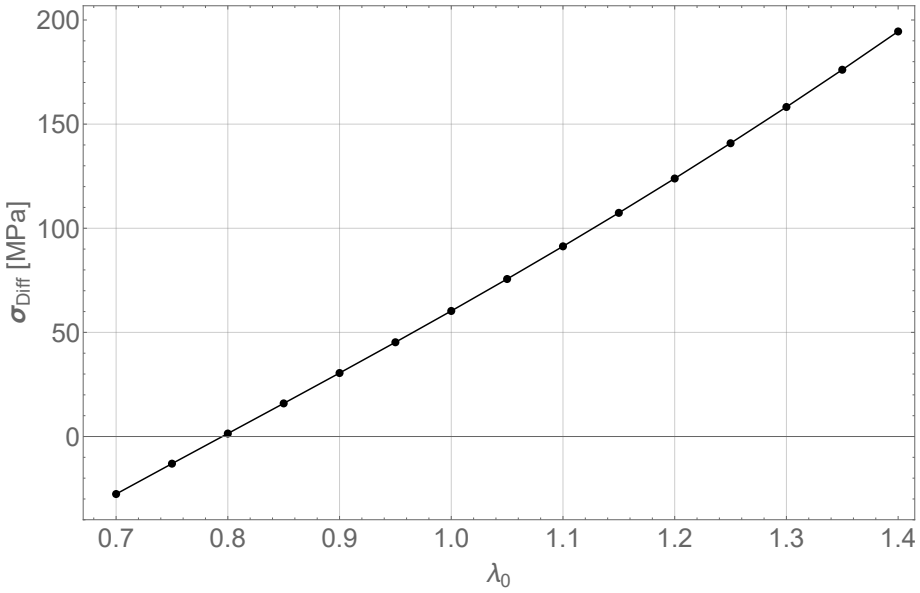

Figure 14: $\boldsymbol{\sigma}_{\text{Diff}} = \boldsymbol{\sigma}_{\text{EE}} - \boldsymbol{\sigma}_{\text{YY}}$ as a function of λ_0 after the removal of the electric field with the magnitude of $E = 150\,\frac{\text{MV}}{m}$.

account and averaging the stresses at $0 \leq \Phi < 2\pi$ with a discretization of $\Delta\Phi = \frac{\pi}{16}$ for each inclination to the electric field, Θ, and evaluating the stresses in each deformation ratio while taking into account the fractions of each inclination (Eq. (116)) in each case of deformation. The mechanical stresses in the direction of the electric field and in the transverse plane as a function of the deformation ratio are presented in Fig. 15 for the isotropic polymer, the biased polymer and the IED model.

The electrostatic properties can be assessed by first evaluating the polarization of the polymer as a function of the magnitude of the electric field. These calculations are performed according to the same steps that were mentioned for the stresses calculations. The susceptibilities of the biased polymer, isotropic polymer and the IED model as a function of the electric field are presented in Fig. 16 as they are calculated according to Eq. (129).

A change in the stresses is visible in Fig. 15 as a result of the presence of an electric field in the polymerization process. More precisely, there is an increase in the stresses of the biased polymer, relatively to the isotropic polymer, in the direction of the electric field and perpendicular to it. The stresses in the IED model are higher than both the other examined polymers.

Fig. 16 shows similar susceptibilities for the biased polymer and the isotropic one. The susceptibilities of both the polymers are as the given initial susceptibility while under the exitation of electric fields with small magnitudes (under $E \cong 5\,\frac{\text{MV}}{\text{m}}$) and they increase in values almost identicaly as the magnitude of the electric field increases. We suspect that the resemblance between the susceptibilities of the biased and isotropic polymers stems from the fact that as the electric field is removed, at the end of our proposed process, the

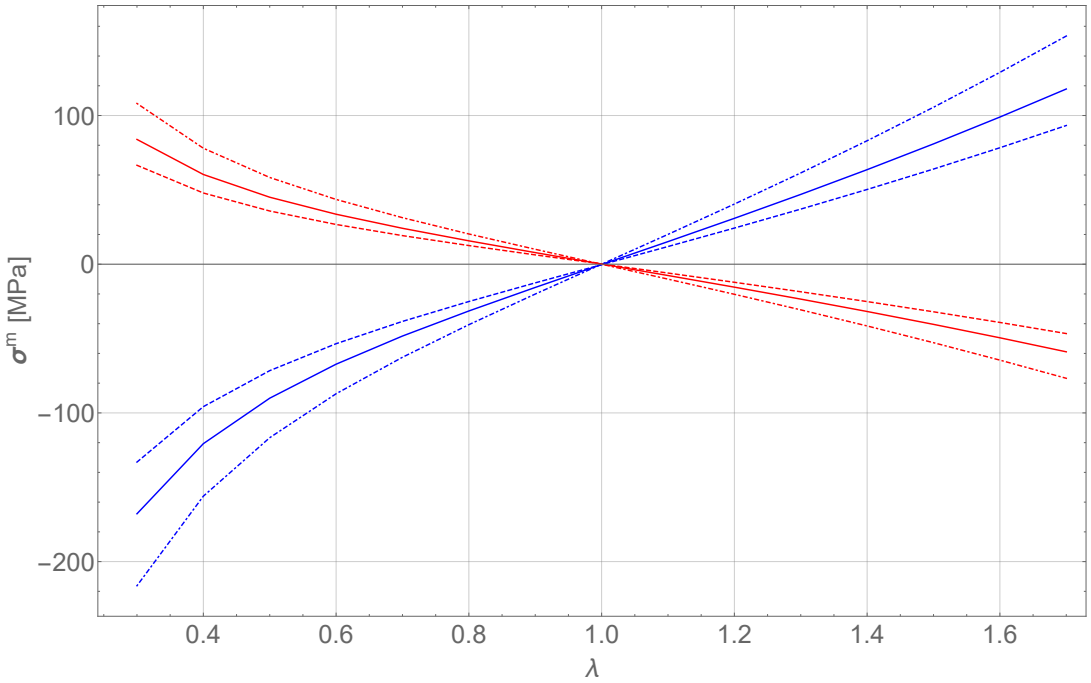

Figure 15: The deviatoric mechanical stress as a function of the deformation ratio, λ. Dashed curves corresponds to the isotropic polymer, continuous curves to the biased polymer and the dot-dashed curves to a polymer described by the IED model. The blue curves corresponds to the normal stress in the direction of the electric field, $\boldsymbol{\sigma}^{\mathrm{m}}_{\mathrm{EE}}$, and the red curves to the transverse stress, $\boldsymbol{\sigma}^{\mathrm{m}}_{\mathrm{YY}} = \boldsymbol{\sigma}^{\mathrm{m}}_{\mathrm{ZZ}}$.

monomers aspire to rearange as in the isotropic case while the biased polymer deforme. We note that the numerical results of the susceptibility for the biased polymer shows a slight increase relatively to the isotropic polymer, though not enough for a visible separation between the curves. The susceptibility of the IED model is not affected by the magnitude of the electric field and is constant in value as the initial susceptibility. Hence, it can be deduced that the changes in the mechanical properties as a result of inducing the polymer with an electric field during the polymerization process are more prominent than those of the electrostatic properties.

4.5 The coupled response

(Note: coupled properties - new polymer + comparison)

After examining and comparing the mechanical and electrostatic properties, the coupled properties of the two mentioned polymers can also be examined. For that purpose, the main criterion to be examined is the deformation, λ, as a function of the magnitude of the induced electric field, presented in Fig. 17. As can be seen in Fig. 17, the deformations of the biased polymer are smaller than those of the isotropic polymer. These results agrees with the previous ones. As it was established from Fig. 16 that the electrostatic response

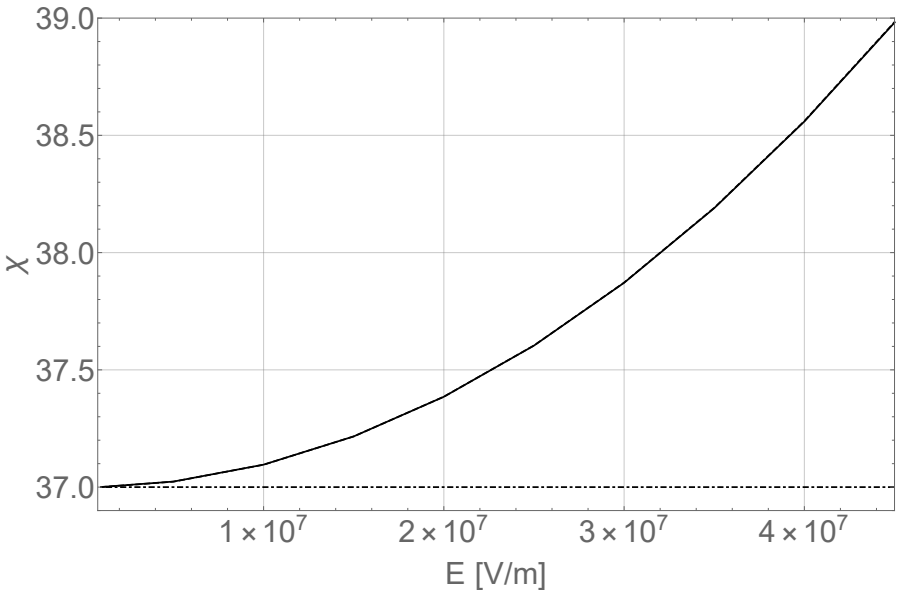

Figure 16: The susceptibilities of the polymers as a function of the electric field. The black dashed curve corresponds to the isotropic polymer, the black continuous curve to the biased polymer and the black dot-dashed line to a polymer described by the IED model. (the dashed and the continuous curves overlap).

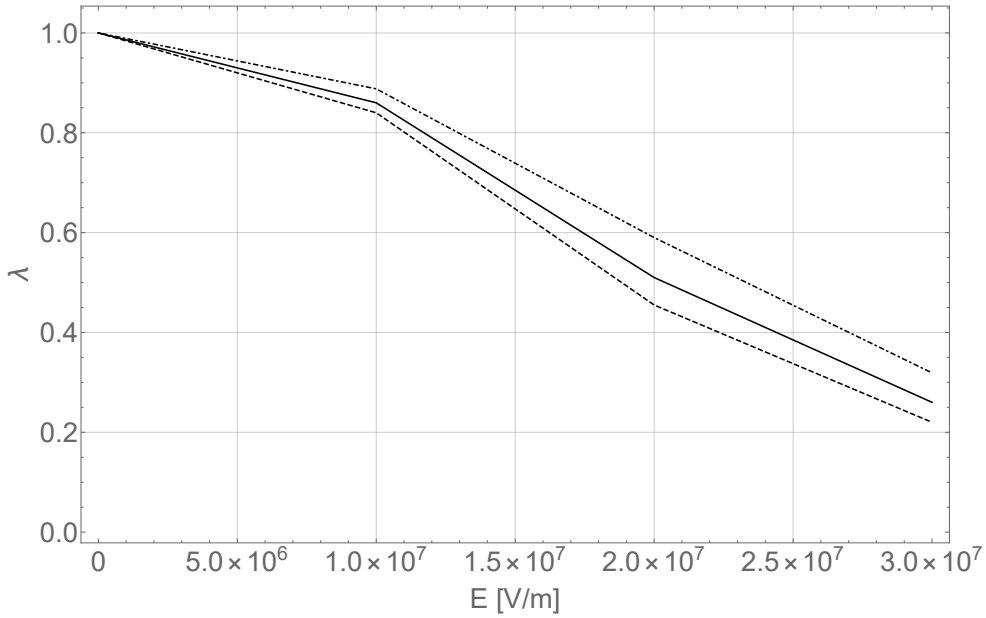

Figure 17: The deformation in the direction of the electric field, λ, as a function of the magnitude of the electric field. The black dashed curve corresponds to the isotropic polymer, the black continuous curve to the biased polymer and the black dot-dashed curves to a polymer described by the IED model.

of the biased polymer shows no meaningful difference from that of the isotropic polymer, from Fig. 15 it can be interpreted that the biased polymer is stiffer than the isotropic polymer. Furthermore, as the susceptibility of the IED model is constant and generally smaller in value than both the other polymers within the examined magnitude range of electric fields, the stresses in the IED model are higher than both the other polymers. Thus, it is logical that the deformations of the IED model are the smallest of the three.

5 Experimental work

Additionally to our analytical and numerical work, as deeper understanding of the polymers coupled electromechanical behavior is required. Experimental studies aimed toward examining the coupled response of different DEs such as VHB and PDMS are also being performed and compared to analytical calculations. The dielectric constant of DEs is determined by firstly determining the capacitance of capacitors with the DEs as their medium, from which the relative permittivity can be calculated. A common method used to carry out such measurements is based on the analysis of the capacitance component in a LCR (L-inductance, C-capacitance, R-resistance) circuit by means of a LCR meter or a simpler versions of this instrument, the capacitance meter.

The presented experimental work is divided to two main parts. The first includes an expansion of the work presented in Cohen et al. [2017] and examines the influence of uniaxial and biaxial stretching on the dielectric constant. The second includes the first presentation of a new experimental system which is aimed towards measuring the dielectric constant of polymers under an electric field. The two polymers that were chosen to be examined are VHB 4910 (a commercially available acrylic elastomer by 3M) and Polydimethylsiloxane (PDMS that was made in our lab from Dow Corning Sylgard 182 Silicone Elastomer Encapsulation Kit). These materials are of interest due to their flexibility and accessibility.

5.1 The influence of uniaxial and biaxial stretching

The first experimental system we present allows us to evaluate the influence of uniaxial and biaxial stretching of DEs on their dielectric constant and deepen the examination of the dependence of the dielectric constant on the deformation. The experimental system is built from a self constructed stretching device with four movable grippers, as can be seen in Fig. 18a. In order to measure the relative permittivity of the deformed samples, a C-shaped clamp is used as a plate capacitor (Fig. 18b) and is connected to a capacitance meter, Agilent U1701A. The experimental relative permittivity of each sample is calculated via

$$\epsilon_{r_{Exp}} = \frac{C_s\, d}{A\, \epsilon_0}, \tag{133}$$

where C_s is the measured capacitance, d and A are the thickness and surface area of the capacitor respectively and ϵ_0 is the vacuum permittivity. The analytical relative permittivity for uniaxial stretch of the dielectric elastomers is calculated via Cohen et al. [2017]

$$\epsilon_{r_U} = 1 + \chi_0 \left(1 - \frac{1}{5\,n}\left(\lambda^2 - \frac{1}{\lambda}\right)\right). \tag{134}$$

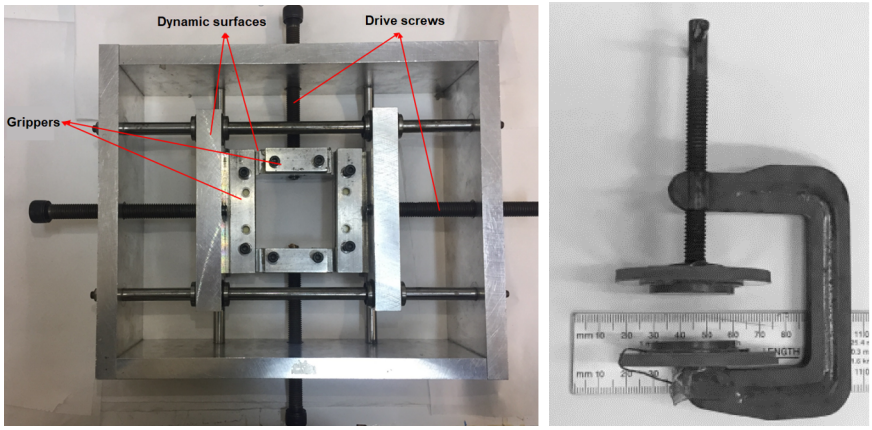

(a) (b)

Figure 18: (a) The self constructed stretching device. (b) The C-clamp used as a parallel plate capacitor.

Table 1: The number of monomers in a single chain for the case presented in Fig. 19.

	PDMS - Uniaxial	VHB - Uniaxial	VHB - Biaxial
n_f	4.35	80	80
n_e	5.844	21.807	5.156

The calculation for the analytical relative permittivity was extracted in the current work from the results of Cohen et al. [2017] to the case of biaxial stretches. The final expression is

$$\epsilon_{r_B} = 1 + \chi_0 \left(1 - \frac{2}{5\,n}\left(\lambda^2 - \frac{1}{\lambda^4}\right)\right), \tag{135}$$

where n is the number of monomers in a single chain, χ_0 is the initial susceptibility and λ is the magnitude of the uniaxial or biaxial stretches.

The results of the experiments and the analytical calculations for the relative permittivity as a function of the percentage of surface area expansion are presented in Fig. 19 for uniaxial stretch of PDMS (Fig. 19a), uniaxial stretch of VHB 4910 (Fig. 19b) and for biaxial stretch of VHB 4910 (Fig. 19c). The analytical results for uniaxial and biaxial stretches are also presented for the different examined cases. The number of monomers in a single chain is estimated from the stretch at failure, which is presumed to be the lock-up stretch, and labeled as n_f and from fitting the analytical equations to the experimental results as n_e, as is shown in Table 1.

As can be observed, while the samples are stretched and their thickness decreases their relative permittivity decreases. The incompressibility assumption was also examined and in the case of the PDMS the results of both the measured and the calculated thickness can be observed. The incompatibility of the curves based on the number of monomers in a polymer chain from the stretch at failure can stem from the fact that the stretch at

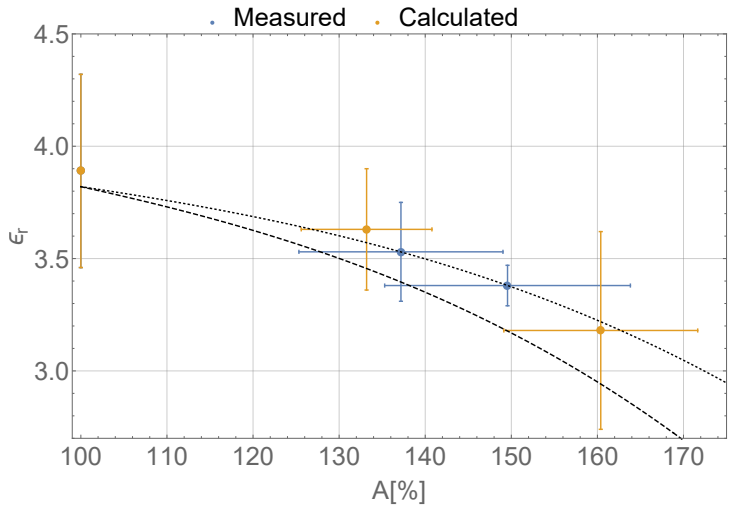

(a)

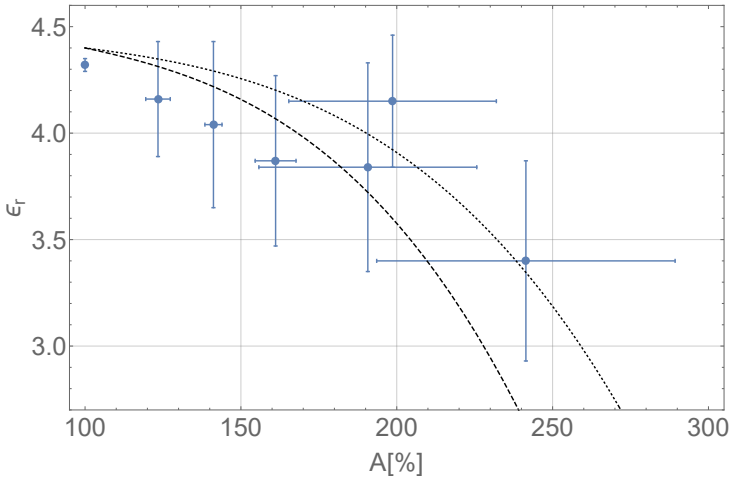

(b)

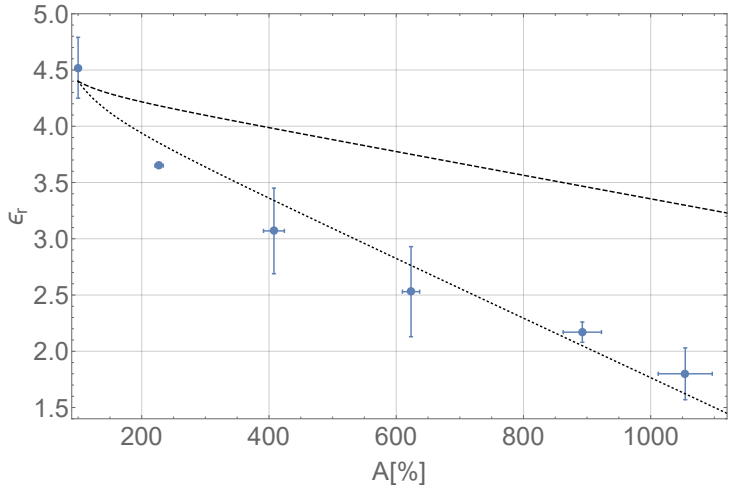

(c)

Figure 19: The relative permittivity measurements as functions of the percentage of surface area expansion. The dashed and dotted curves correspond to the analytical results [Cohen et al., 2017], as n are estimated from the stretch at failure (n_f) and from fitting the analytical equations to the experimental results (n_e), respectively. (a) PDMS under uniaxial stretch. (b) VHB under uniaxial stretch. (c) VHB under biaxial stretch.

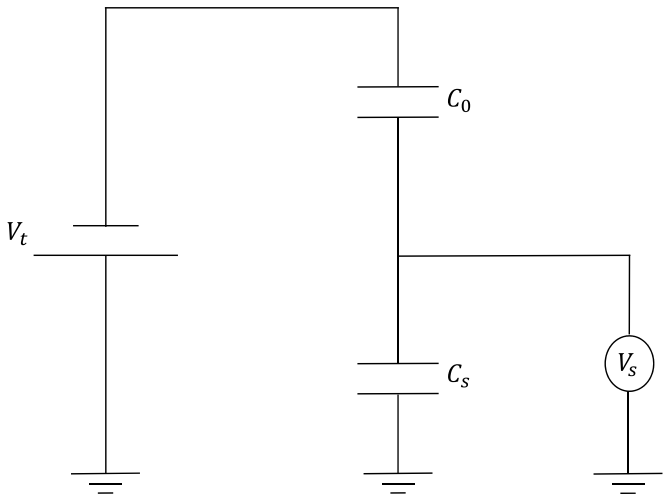

Figure 20: A schematic description of the experimental system.

failure is not necessarily the lock-up stretch of the chain.

5.2 The influence of an electric field

This experimental work is aimed toward examining the effect of electric fields with different magnitudes on the dielectric properties of various polymers. For that purpose, we will present a new experimental system which allows us to evaluate the variations of the dielectric constant as an electric field is applied on them. Furthermore, we will continue the work performed in Cohen et al. [2017] and deepen the examination of the dependence of the dielectric constant on the deformation by performing our examination on pre-stretched samples.

5.2.1 Experimental set-up

(Note: Samples description)

(Note: Presenting the experimental system)

Ten rectangular samples of each of the two chosen polymers were cut for each examined case. For the case of the pre-stretched VHB, the samples were then stretched using a self constructed stretching apparatus comprised of two movable grippers, as can be seen in Fig. 18a.

Our new experimental system is built from non-conductive materials, all but the two electrodes with a diameter of 30 mm that are made from copper and acts as one of two capacitors connected in a row, as can be seen in Fig. 20. The two electrodes are each held in a Teflon housing with a 60 mm diameter, as can be seen in Fig 21. As the medium in

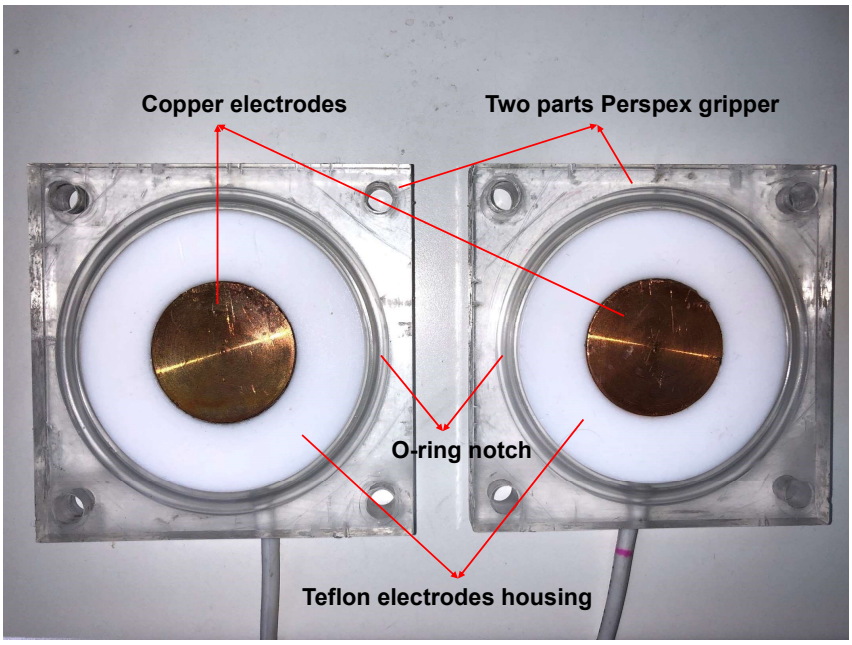

Figure 21: The parts of the plate capacitore.

the mentioned plate capacitor is the examined elastomer sample, the second capacitor is a capacitor with a fixed capacitance, which can be regarded as a fixed capacitor. For the current work a ceramic capacitor suitable for high voltage is used, TDK's UHV-241A.

For the case of examining pre-stretched samples we first use a bi-directional stretching apparatus in order to generate the required tension. After the stretching the sample is held in the stretched state using a two parts self constructed Perspex gripper with an opening of 60 mm diameter in the middle and an O-ring notch to maintain the tension in the sample, as can be seen in Fig. 21.

In order to measure the referential permittivity of the different samples, we make use of the plate capacitor from our experimental system. This measurement is performed by connecting it to a capacitance meter before the experimental system is connected to the power source. Furthermore, the distance between the electrodes is measured in each experiment. After the referential values are obtained, the power source is connected to the described system. As the supplied potential difference is changed in the power source the potential difference on the plate capacitor is measured by a non-contact voltmeter, USSVM2 by AlphaLab.

(Note: Presenting the work method or protocol)

For the purpose of evaluating the relative permittivity of the polymer while under an electrostatic excitation the charge conservation is taken into account,

$$Q = C_s V_s = C_0 V_0, \tag{136}$$

where Q is the charge on both of the capacitors, V_s and C_s are the potential difference

and the capacitance of the examined polymer and V_0 and C_0 are the potential difference and the capacitance of the fixed capacitor. Thus,

$$V_t = V_s + V_0 = Q\left(\frac{1}{C_s} + \frac{1}{C_0}\right), \tag{137}$$

where V_t is the total potential difference as it is supplied from the power source. While taking into account Eq. (137) we can obtain the relation,

$$C_s = \left(\frac{V_t}{V_s} - 1\right) C_0, \tag{138}$$

from which the current capacitance of the polymer can be calculated, while the constant value of C_0 is taken from its data shit and confirmed at the beginning of the experiment with the capacitance meter.

The relative permittivity, which is the electrostatic property that we aim to examine, is calculated from the results of the capacitance calculations by using the relationes presented in Eq. (133).

5.2.2 Results and discussion

In all test the thickness of the samples were measured for the calculation of the relative permittivity, presented in Eq. (133), and the correct assessment of the electric field that is induced on the sample, which is calculated as $E_s = \frac{V_s}{d}$. Measuring the pre-stretched VHB 4910 have led to the understanding that the incompressibility assumption is reasonable and can be employed in this case.

In the two plots of Fig. 22, the relative permittivity measurements as functions of the electric field on the samples for the un-stretched samples are marked by blue filled dots and for the 2.25 area pre-stretched samples by red empty circles. The standard deviations are marked by error bars. An agreement between the results shown in section 5.1 and the current results can be identified in cases where $E_s \to 0$. In the case of the VHB 4910 samples (Fig. 22b), the relatively small standard deviations of the different measurements provide confidence in the accuracy of the measurements for this material. The relatively larger standard deviations of the PDMS samples can be as a result of the fact that the samples were made manually in our lab, although there is a clear trend in the results. We find that the relative permittivity of the two examined polymers increase with the magnitude of the electric field.

The variations in the responses of the two examined polymers hints that these are governed by the microstructure of the polymers. Furthermore, another evidence to the governing of the microstructure can be seen in the results of the pre-stretched VHB 4910.

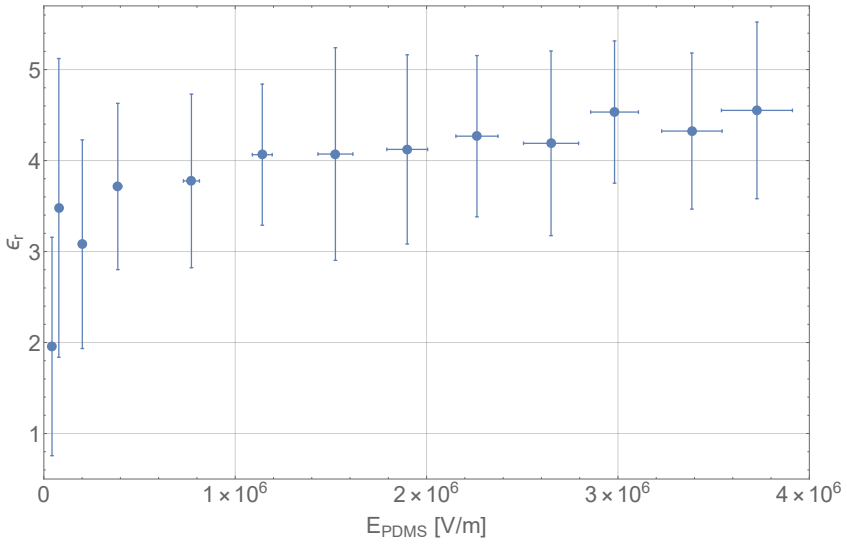

(a)

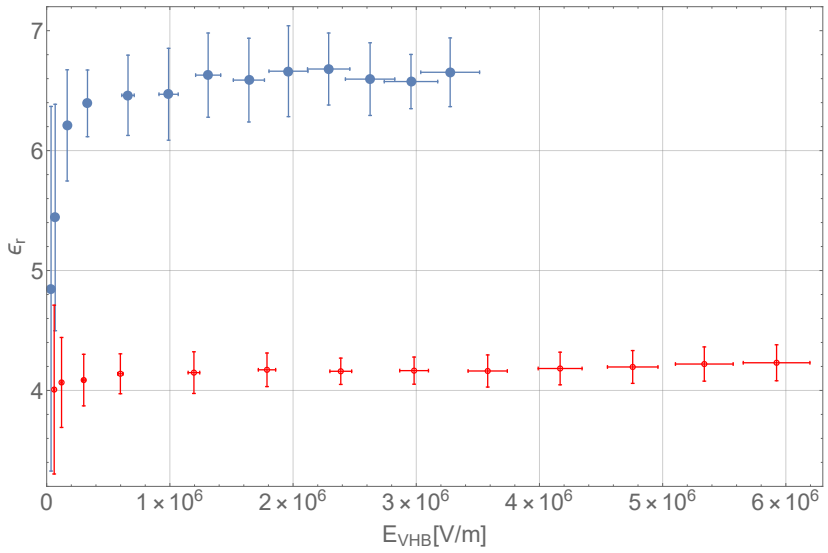

(b)

Figure 22: The permittivity measurements a functions of the electric field on the sample. The Blue dots corresponds to a relaxed sample and the red circles corresponds to the area pre-stretch of $A = 225\%$. (a) PDMS, (b) VHB.

As the initial values of the relative permittivity correspond to the results in Fig. 19, the maximum relative permittivity measured in the pre-stretched case is much lower then the one measured in the relaxed case despite the fact that we achived larger magnituds of electric field as the thickness of the samples was decreased. It can be seen in the results for both the polymers (Fig. 22), the relative permittivity deviation is much steeper in relative low electric fields ($< 1\frac{\mathrm{MV}}{\mathrm{m}}$). Thus, additional experimental analyses of the relations between the microscopic structure and the macroscopic response are needed for the understanding of the coupled electromechanical behaviors of different polymers.

6 Conclusions

(Note: Opening - Motivation)

Although this thesis presents another possible step towards the realization of the DEs potential for being used in a wide range of applications, it comes at a time when our culture is seemingly ready for such advances in different fields such as clean energy, medicine and robotics. Hence, as a substantial improvement in the electromechanical response of DEs is needed, we present a possible method for influencing and analysing the response, structure and properties of the polymer, all without adding any foreign materials.

(Note: 3. Electroelasticity of solutions and anisotropic networks of polymer molecules)

(Note: 3.1 general - multiscale analysis)

Initially, we carried out a multiscale analysis of the electromechanical coupling in DEs at several hierarchical cases, from a single electric charge to a network. The analysis accounts for the conservation of energy through the first law of thermodynamics, in terms of the electric enthalpy and the entropy of a system that is subjected to an electric field. Our analysis of the microstructure of the polymer is based on statistical mechanics as we assume that the configuration of each chain is the one that was calculated as most probable.

(Note: 3.2 an analysis of the isotropic chain end-to-end length, tau and force)

We carry out an analysis of the polymer chain, in the case of no electric field. This analysis yielded the relations between the Lagrange multiplier τ, which can be portrayed as the chain's mechanical constraint, and the normalized end-to-end length of the chain through the Langevin function. Our calculations also yielded an assessment for the end-to-end length of a chain in such a case, which is similar to the one obtained by Flory [1949, 1953] and Treloar [1975] but different than the commonly used assessment given from random walk statistics [Kuhn, 1934, Treloar, 1973, Arruda and Boyce, 1993]. A relation between the end-to-end length of a chain and the external force operating on it was also deduced.

(Note: 3.3 polymer chains in an electric field and monomers distribution)

As our proposed method for controlling the electroelastic moduli of a network by executing the polymerization process under an electric field is examined, we describe a manner for the assessment of the most probable configurations for each of the chains groups and for the monomers orientational distribution in such a case.

(Note: 3.4 an anisotropic network analysis - general analysis with a reference for polymerization under an electric field + material properties)

Next, an expression is derived for the total entropy of the polymer which allows us to evaluate the distribution and the fractions of the chains in the different chains groups. Next, once the fractions of the chains in the different groups were determined, expressions

for the mechanical stress and the polarization were derived in order to determine the response of the polymer.

(Note: 4. Application to electrostatically biased network - remined our main idea for the polymerization**)**

To examine the outcome of our proposed process of polymerization under an electric field, that leads to a "biased" polymer, a numerical analysis was performed. This analysis is an application of our analytical work, and its prediction is compared with the results for an isotropic polymer and the IED model.

(Note: 4.1 chain end-to-end length - isotropic case (our analysis is more accurate) and anisotropic (mention the examined parameters)**)**

The initial step of the numerical analysis involved an examination of our assessment for the end-to-end length of a chain in the case of an isotropic polymer. In regards to the configuration of the chains in the biased polymer, a comparison was performed for three parameters: the maximum number of configurations of the chain, the most probable end-to-end length and the Lagrange multiplier $\boldsymbol{\tau}$ that relates to the end-to-end length with the maximum number of configurations. From which we determined that magnitude ranges of electric fields lower than $50\,\frac{\mathrm{MV}}{\mathrm{m}}$ have shown hardly any differences in results from the isotropic case. Though, when enhancing the magnitude furthur, the end-to-end length of chains in all inclinations increases, which is counterintuitive as the uniaxial dipolar monomers aspire to rotate towards the direction of the electric exitation.

(Note: 4.2 monomer orientation - aspire to be as in the amorphous case**)**

The findings from the examinations of the monomers orientation for chains in the different inclinations and the comparison to the distribution of monomers in the amorphous case led to the realization that despite their constraints, the monomers in the chains aspire to orient as though they are unattached.

(Note: 4.3 assessing the free state and discussing the chains distribution/weights**)**

Next, the free state of the biased polymer was assessed. This state is achieved when the deviatoric stress vanishes and the body is at a stress free configuration. It was found that the biased polymer contracts in the direction of the applied electric field. This strengthens our understanding of the importance of the microscopic structure to the properties of the polymer, since when the electric field is turned off the monomers rotate away from its direction and hence the contraction in that direction. The spatial expansion in the transverse direction is due to incompressibility.

(Note: 4.4 the material properties and coupled response**)**

The resulting material properties shows a difference between the mechanical ones as the biased polymer is found to be stiffer than the isotropic one. Regarding the electrostatic properties, no significant differences were found between the two polymers. Though, in both cases the susceptibility does not appear to be fixed under different magnitudes of

electric fields. In accordance with the assessed mechanical and electrostatic properties of both polymers, from the analysis of the coupled response, it was established that the electromechanical response of the biased polymer is smaller then the isotropic polymer.

(Note: 5. Experimental work)

The findings of our experimental work imply that the dependence of the polymers dielectric properties on the deformation and the magnitude of the electric field cannot be neglected. Moreover, they suggest that common models that assume constant relative permittivity, such as the models of Wissler and Mazza [2007] and Dorfmann and Ogden [2017], are not applicable if the polymer is subjected to different mechanical loads or excitations from electric fields at different magnitudes. Additionally, we observed that our extension to the model of Cohen et al. [2017] for the case of biaxial stretches is able to predict the relations between the relative permittivity, which represents the dielectric behavior, and the deformation of the polymer. Though, the assessment of the number of monomers in a single chain from the stretch at failure does not yield a good enough prediction of the mentioned relations. This can stem from the fact that the stretch at failure is not necessarily the lock-up stretch of the chain. Furthermore, from our examination of the effect of electric fields with different magnitudes on the dielectric properties, the differences in the responses of the relaxed and pre-stretched VHB 4910 demonstrate the prominent influence of the microscopic structure on the macroscopic electromechanical behavior. Accordingly, it can be seen that pre-stretching the sample hinders the evolution of the relative permittivity as the magnitude of the electric field increases.

(Note: ** Future work)

We have spent considerable time pondering the future directions of this research. While this thesis presented a method of influencing the properties of polymers, so far it was applied only to the case of uniaxial dipoles. Thus, an analysis should be performed for spontaneous and transversely isotropic dipoles as well. Additionally, the creation of a biased polymer should be examined from different directions and with greater magnitudes of electric fields in order to assess the threshold field from which there are segnificent differences in the electrostatic properties in comparison with the isotropic polymer. Moreover, from the experimental perspective, the influence of an electric field on the dielectric properties should be examined for additional materials, with more pre-stretching conditions and under higher magnitudes of electric fields.

References

Z. Ahmad. Polymeric dielectric materials. *Dielectric Material*, 2012.

E. M. Arruda and M. C. Boyce. A three-dimensional constitutive model for the large stretch behavior of rubber elastic materials. *Journal of the Mechanics and Physics of Solids*, 41(2):389 – 412, 1993. ISSN 0022-5096.

A. Barnes, Q. Liu, and T.-F. Young, G.and Lu. Evaluation of selected dielectric elastomers for use in an artificial muscle actuator. In *Proceedings of the Australasian Conference on Robotics and Automation*, pages 1–9. Citeseer, 2007.

T. Blythe and D. Bloor. *Electrical properties of polymers*. Cambridge university press, 2005.

R. A. Bustamante. Transversely isotropic non-linear electro-active elastomers. *Acta Mechanica*, 206(3):237, Oct 2008. ISSN 1619-6937.

F. Carpi, D. De Rossi, R. Kornbluh, R. E. Pelrine, and P. Sommer-Larsen. *Dielectric elastomers as electromechanical transducers: Fundamentals, materials, devices, models and applications of an emerging electroactive polymer technology*. Elsevier, 2011.

H. R. Choi, K. Jung, N. H. Chuc, M. Jung, I. Koo, J. Koo, J. Lee, J. Lee, J. Nam, M. Cho, et al. Effects of prestrain on behavior of dielectric elastomer actuator. In *Smart structures and materials*, pages 283–291. International Society for Optics and Photonics, 2005.

N. Cohen and G. deBotton. Multiscale analysis of the electromechanical coupling in dielectric elastomers. *European Journal of Mechanics-A/Solids*, 48:48–59, 2014.

N. Cohen and G. deBotton. The electromechanical response of polymer networks with long-chain molecules. *Mathematics and Mechanics of Solids*, 20(6):721–728, 2015.

N. Cohen and G. deBotton. Electromechanical interplay in deformable dielectric elastomer networks. *Physical review letters*, 116(20):208303, 2016.

N. Cohen, K. Dayal, and G. deBotton. Electroelasticity of polymer networks. *Journal of the Mechanics and Physics of Solids*, 92:105 – 126, 2016. ISSN 0022-5096.

N. Cohen, S. S. Oren, and G. deBotton. The evolution of the dielectric constant in various polymers subjected to uniaxial stretch. *Extreme Mechanics Letters*, 16:1 – 5, 2017. ISSN 2352-4316.

B. D. Coleman and W. Noll. The thermodynamics of elastic materials with heat conduction and viscosity. *Archive for Rational Mechanics and Analysis*, 13(1):167–178, 1963.

G. deBotton. private communication. 2020.

G. deBotton, L. Tevet-Deree, and E. A. Socolsky. Electroactive heterogeneous polymers: analysis and applications to laminated composites. *Mechanics of Advanced Materials and Structures*, 14(1):13–22, 2007.

L. Di Lillo, A. Schmidt, D. A. Carnelli, P. Ermanni, G. Kovacs, E. Mazza, and A. Bergamini. Measurement of insulating and dielectric properties of acrylic elastomer membranes at high electric fields. *Journal of Applied Physics*, 111(2):024904, 2012.

A. Dorfmann and W. R. Ogden. Nonlinear electroelasticity. *Acta Mechanica*, 174(3): 167–183, 2005. ISSN 1619-6937.

L. Dorfmann and R. W. Ogden. Nonlinear electroelasticity: material properties, continuum theory and applications. *473 Proc. R. Soc. A.*, 2017.

A. Cemal Eringen. On the foundations of electroelastostatics. *International Journal of Engineering Science*, 1(1):127 – 153, 1963. ISSN 0020-7225.

P. J. Flory. The configuration of real polymer chains. *The Journal of Chemical Physics*, 17(3):303–310, 1949.

P. J. Flory. *Principles of polymer chemistry*. Cornell University Press, 1953.

P. J. Flory and J. Rehner. Statistical mechanics of cross linked polymer networks i. rubberlike elasticity. *The Journal of Chemical Physics*, 11(11):512–520, 1943.

G. Y. Gu, J. Zhu, L. M. Zhu, and X. Zhu. A survey on dielectric elastomer actuators for soft robots. *Bioinspiration & biomimetics*, 12(1):011003, 2017.

C. Huang, Q. M. Zhang, K. Bhattacharya, et al. All-organic dielectric-percolative three-component composite materials with high electromechanical response. *Applied Physics Letters*, 84(22):4391–4393, 2004.

K. Hutter, A. A. F. Ven, and A. Ursescu. *Electromagnetic Field Matter Interactions in Thermoelastic Solids and Viscous Fluids*, volume 710. Springer, 2007.

H. M. James and E. Guth. Statistical thermodynamics of rubber elasticity. *The Journal of Chemical Physics*, 21(6):1039–1049, 1953.

S. M. A. Jimenez and R. M. McMeeking. Deformation dependent dielectric permittivity and its effect on actuator performance and stability. *International Journal of Non-Linear Mechanics*, 57:183 – 191, 2013. ISSN 0020-7462.

K. Jung, J. C. Koo, Y. K. Lee, H. R. Choi, et al. Artificial annelid robot driven by soft actuators. *Bioinspiration & biomimetics*, 2(2):S42, 2007.

N. Kellaris, V. Gopaluni Venkata, G. M. Smith, S. K. Mitchell, and C. Keplinger. Peano-hasel actuators: Muscle-mimetic, electrohydraulic transducers that linearly contract on activation. *Science Robotics*, 3(14), 2018.

G. Kofod, P. Sommer-Larsen, R. Kornbluh, and R. Pelrine. Actuation response of polyacrylate dielectric elastomers. *Journal of intelligent material systems and structures*, 14(12):787–793, 2003.

G. Kofod, H. Stoyanov, M. Kollosche, S. Risse, H. Ragusch, D. N. McCarthy, R. Waché, D. Rychkov, and M. Dansachmüller. Molecular level materials design for improvements of actuation properties of dielectric elastomer actuators. In *SPIE Smart Structures and Materials+ Nondestructive Evaluation and Health Monitoring*, pages 79760J–79760J. International Society for Optics and Photonics, 2011.

W. Kuhn. Über die gestalt fadenförmiger moleküle in lösungen. *Kolloid-Zeitschrift*, 68 (1):2–15, 1934.

W. Kuhn and F. Grün. Beziehungen zwischen elastischen konstanten und dehnungsdoppelbrechung hochelastischer stoffe. *Kolloid-Zeitschrift*, 101(3):248–271, December 1942. ISSN 1435-1536.

B. Kussmaul, S. Risse, G. Kofod, R. Waché, M. Wegener, D. N. McCarthy, H. Krüger, and R. Gerhard. Enhancement of dielectric permittivity and electromechanical response in silicone elastomers: molecular grafting of organic dipoles to the macromolecular network. *Advanced Functional Materials*, 21(23):4589–4594, 2011.

O. Lopez-Pamies. Elastic dielectric composites: Theory and application to particle-filled ideal dielectrics. *Journal of the Mechanics and Physics of Solids*, 64:61 – 82, 2014. ISSN 0022-5096.

T. Lu, J. Huang, C. Jordi, G. Kovacs, R. Huang, D. R. Clarke, and Z. Suo. Dielectric elastomer actuators under equal-biaxial forces, uniaxial forces, and uniaxial constraint of stiff fibers. *Soft Matter*, 8(22):6167–6173, 2012.

F. B. Madsen, A. E. Daugaard, S. Hvilsted, and A. L. Skov. The current state of silicone-based dielectric elastomer transducers. *Macromolecular Rapid Communications*, 2016.

R. M. McMeeking and C. M. Landis. Electrostatic forces and stored energy for deformable dielectric materials. *Journal of Applied Mechanics, Transactions ASME*, 72(4):581–590, 7 2005. ISSN 0021-8936.

R. M. McMeeking, C. M. Landis, and S. M. A. Jimenez. A principle of virtual work for combined electrostatic and mechanical loading of materials. *International Journal of Non-Linear Mechanics*, 42(6):831 – 838, 2007. ISSN 0020-7462.

M. Moscardo, X. Zhao, Z. Suo, and Y. Lapusta. On designing dielectric elastomer actuators. *Journal of Applied Physics*, 104(9):093503, 2008.

R. W. Ogden. *Non-linear elastic deformations*. Dover Publications, Mineola, N.Y., 1997. ISBN 9780486696485.

R. Pelrine, R. Kornbluh, Q. Pei, and J. Joseph. High-speed electrically actuated elastomers with strain greater than 100%. *Science*, 287(5454):836–839, 2000.

J.-S. Plante and S. Dubowsky. Large-scale failure modes of dielectric elastomer actuators. *International journal of solids and structures*, 43(25):7727–7751, 2006.

J.-S. Plante and S. Dubowsky. On the properties of dielectric elastomer actuators and their design implications. *Smart Materials and Structures*, 16(2):S227–S236, mar 2007.

J. Qiang, H. Chen, and B. Li. Experimental study on the dielectric properties of polyacrylate dielectric elastomer. *Smart Materials and Structures*, 21(2):025006, 2012.

P. Rothemund, N. Kellaris, and C. Keplinger. How inhomogeneous zipping increases the force output of peano-hasel actuators. *Extreme Mechanics Letters*, 31:100542, 2019. ISSN 2352-4316.

S. Rudykh, A. Lewinstein, G. Uner, et al. Analysis of microstructural induced enhancement of electromechanical coupling in soft dielectrics. *Applied Physics Letters*, 102(15): 151905, 2013.

D. Rus and M. T. Tolley. Design, fabrication and control of soft robots. *Nature*, 521 (7553):467–475, 2015.

W. H. Stockmayer. Dielectric dispersion in solutions of flexible polymers. *Pure and Applied Chemistry*, 15(3-4):539–554, 1967.

H. Stoyanov, M. Kollosche, D. N. McCarthy, and G. Kofod. Molecular composites with enhanced energy density for electroactive polymers. *Journal of Materials Chemistry*, 20(35):7558–7564, 2010.

T. Su and P. K. Purohit. Semiflexible filament networks viewed as fluctuating beam-frames. *Soft Matter*, 8:4664–4674, 2012.

L. Tian, L. Tevet-Deree, G. deBotton, and K. Bhattacharya. Dielectric elastomer composites. *Journal of the Mechanics and Physics of Solids*, 60(1):181–198, 2012.

H. F. Tiersten. *A development of the equations of electromagnetism in material continua.* 1990.

R. A. Toupin. The elastic dielectric. *J. Ration. Mech. Anal.*, 5:849–915, 1956. ISSN 1943-5282.

L. R. G. Treloar. The elasticity of a network of long-chain molecules. i. *Trans. Faraday Soc.*, 39:36–41, 1943.

L. R. G. Treloar. The elasticity and related properties of rubbers. *Reports on progress in physics*, 36(7):755, 1973.

L. R. G. Treloar. *The physics of rubber elasticity.* Monographs on the Physics and Chemistry of Materials. Clarendon Press, 1975.

J. D. Vogan. *Development of dielectric elastomer actuators for MRI devices.* PhD thesis, Massachusetts Institute of Technology, 2004.

Valentina Volpini, Lorenzo Bardella, and Massimiliano Gei. A note on the solution of the electro-elastic boundary-value problem for rank-two laminates at finite strains. *Meccanica*, 54(13):1971–1982, 2019.

F. T. Wall and P. J. Flory. Statistical thermodynamics of rubber elasticity. *The Journal of Chemical Physics*, 19(12):1435–1439, 1951.

M. C. Wang and E. Guth. Statistical theory of networks of non-gaussian flexible chains. *The Journal of Chemical Physics*, 20(7):1144–1157, 1952.

M. Warner and E. M. Terentjev. *Liquid Crystal Elastomers.*, volume Rev. ed of *International Series of Monographs on Physics.* OUP Oxford, 2003.

M. Wissler and E. Mazza. Electromechanical coupling in dielectric elastomer actuators. *Sensors and Actuators A: Physical*, 138(2):384 – 393, 2007. ISSN 0924-4247.

L. Xu, H. Q. Chen, J. Zou, W. T. Dong, G. Y. Gu, L. M. Zhu, and X. Y. Zhu. Bio-inspired annelid robot: a dielectric elastomer actuated soft robot. *Bioinspiration & Biomimetics*, 12(2):025003, jan 2017.

Q. M. Zhang, J. Su, C. H. Kim, R. Ting, and R. Capps. An experimental investigation of electromechanical responses in a polyurethane elastomer. *Journal of Applied Physics*, 81(6):2770–2776, 1997.

X. Zhao and Z. Suo. Electrostriction in elastic dielectrics undergoing large deformation. *Journal of Applied Physics*, 104(12):123530, 2008.

Appendix

A Presentation of the first law of thermodynamics in terms of electrical enthalpy

The first law of thermodynamics is $\dot{U} = \dot{W}_0 + \dot{Q}$ (Eq. (7)) [McMeeking and Landis, 2005, deBotton et al., 2007] where

$$\dot{U} = \frac{\mathrm{d}}{\mathrm{d}t}\int_{V_0} u\left(\boldsymbol{F}, \mathbf{P}\right) \mathrm{d}V_0 + \frac{\mathrm{d}}{\mathrm{d}t}\int_{\mathbb{R}^3} \frac{\epsilon_0}{2}\mathbf{E}\cdot\mathbf{E}\mathrm{d}V, \tag{139}$$

and where no interactions between the system and other bodies and that far away the electric fields vanish are assumed. The work done the mechanical loads due to deformation and by the electric field due to variations in the charge [McMeeking and Landis, 2005, deBotton et al., 2007]

$$\frac{\mathrm{d}W_0}{\mathrm{d}t} = \int_V b_i v_i \,\mathrm{d}V + \int_{\partial V} t_i v_i \,\mathrm{d}A + \int_V \phi \frac{\mathrm{d}}{\mathrm{d}t}\left(q \,\mathrm{d}V\right) + \int_{\partial V} \phi \frac{\mathrm{d}}{\mathrm{d}t}\left(\rho_a \,\mathrm{d}A\right). \tag{140}$$

We recall the definition of the electric enthalpy density [Cohen et al., 2016]

$$h\left(\boldsymbol{F}, \mathbf{E}\right) = u\left(\boldsymbol{F}, \mathbf{P}\right) - J\mathbf{P}\cdot\mathbf{E}. \tag{141}$$

Accordingly

$$\begin{aligned}\dot{U} &= \frac{\mathrm{d}}{\mathrm{d}t}\int_{V_0} h\left(\boldsymbol{F}, \mathbf{E}\right)\mathrm{d}V_0 + \frac{\mathrm{d}}{\mathrm{d}t}\int_{V_0} \mathbf{P}\cdot\mathbf{E}J\mathrm{d}V_0 + \frac{\mathrm{d}}{\mathrm{d}t}\int_{\mathbb{R}^3}\frac{\epsilon_0}{2}\mathbf{E}\cdot\mathbf{E}\mathrm{d}V \\ &= \frac{\mathrm{d}}{\mathrm{d}t}\int_{V_0} h\left(\boldsymbol{F}, \mathbf{E}\right)\mathrm{d}V_0 + \frac{\mathrm{d}}{\mathrm{d}t}\int_{V} \mathbf{P}\cdot\mathbf{E}\mathrm{d}V + \frac{\mathrm{d}}{\mathrm{d}t}\int_{\mathbb{R}^3}\frac{\epsilon_0}{2}\mathbf{E}\cdot\mathbf{E}\mathrm{d}V.\end{aligned} \tag{142}$$

Since in the body $\mathbf{D} = \mathbf{P} + \epsilon_0\mathbf{E}$ and outside the body $\mathbf{D} = \epsilon_0\mathbf{E}$

$$\dot{U} = \frac{\mathrm{d}}{\mathrm{d}t}\int_{V_0} h\left(\boldsymbol{F}, \mathbf{E}\right)\mathrm{d}V_0 + \frac{\mathrm{d}}{\mathrm{d}t}\int_{\mathbb{R}^3} \left(\mathbf{D} - \epsilon_0\mathbf{E}\right)\cdot\mathbf{E}\mathrm{d}V + \frac{\mathrm{d}}{\mathrm{d}t}\int_{\mathbb{R}^3}\frac{\epsilon_0}{2}\mathbf{E}\cdot\mathbf{E}\mathrm{d}V. \tag{143}$$

Thus, we have that

$$\dot{U} = \frac{\mathrm{d}}{\mathrm{d}t}\int_{V_0} h\left(\boldsymbol{F}, \mathbf{E}\right)\mathrm{d}V_0 - \frac{\mathrm{d}}{\mathrm{d}t}\int_{\mathbb{R}^3}\frac{\epsilon_0}{2}\mathbf{E}\cdot\mathbf{E}\mathrm{d}V + \frac{\mathrm{d}}{\mathrm{d}t}\int_{\mathbb{R}^3} \mathbf{D}\cdot\mathbf{E}\mathrm{d}V. \tag{144}$$

Define $\dot{H} = \frac{\mathrm{d}}{\mathrm{d}t}\int_{\Omega_0} h\left(\boldsymbol{F}, \mathbf{E}\right)\mathrm{d}V_0$ as the stored electric enthalpy in the body. According

to the first law of thermodynamics

$$\dot{H} - \frac{\mathrm{d}}{\mathrm{d}t}\int_{\mathbb{R}^3} \frac{\epsilon_0}{2}\mathbf{E}\cdot\mathbf{E}\mathrm{d}V = \dot{W}_0 + \dot{Q} - \frac{\mathrm{d}}{\mathrm{d}t}\int_{\mathbb{R}^3} \mathbf{D}\cdot\mathbf{E}\mathrm{d}V. \tag{145}$$

Consider the last term

$$-\frac{\mathrm{d}}{\mathrm{d}t}\int_{\mathbb{R}^3} \mathbf{D}\cdot\mathbf{E}\mathrm{d}V = \frac{\mathrm{d}}{\mathrm{d}t}\int_{\mathbb{R}^3} \mathbf{D}\cdot\nabla\phi\mathrm{d}V = \frac{\mathrm{d}}{\mathrm{d}t}\int_{\mathbb{R}^3} \nabla\cdot(\mathbf{D}\phi)\,\mathrm{d}V - \frac{\mathrm{d}}{\mathrm{d}t}\int_{\mathbb{R}^3} \nabla\cdot\mathbf{D}\phi\mathrm{d}V. \tag{146}$$

Assuming no free charges outside the body, then $\nabla\cdot\mathbf{D} = q$ in the body and zero outside,

$$-\frac{\mathrm{d}}{\mathrm{d}t}\int_{\mathbb{R}^3} \mathbf{D}\cdot\mathbf{E}\mathrm{d}V = \frac{\mathrm{d}}{\mathrm{d}t}\int_{\partial V} \phi\mathbf{D}\cdot\hat{\mathbf{n}}\mathrm{d}A - \frac{\mathrm{d}}{\mathrm{d}t}\int_{V} \phi q\mathrm{d}V, \tag{147}$$

where we make use of the divergence theorem and exploit the assumption that far enough the electric field vanish. Thus,

$$-\frac{\mathrm{d}}{\mathrm{d}t}\int_{\mathbb{R}^3} \mathbf{D}\cdot\mathbf{E}\mathrm{d}V = -\frac{\mathrm{d}}{\mathrm{d}t}\int_{\partial V} \phi\rho_a\mathrm{d}A - \frac{\mathrm{d}}{\mathrm{d}t}\int_{V} \phi q\mathrm{d}V. \tag{148}$$

The last term can be simplified to

$$\begin{aligned} -\frac{\mathrm{d}}{\mathrm{d}t}\int_V \phi q\mathrm{d}V &= -\frac{\mathrm{d}}{\mathrm{d}t}\int_{V_0} \phi q J\mathrm{d}V_0 = -\int_{V_0} \dot{\phi} q J\mathrm{d}V_0 - \int_{V_0} \phi\frac{\mathrm{d}}{\mathrm{d}t}\left(qJ\,\mathrm{d}V_0\right) \\ &= -\int_V \dot{\phi} q\mathrm{d}V - \int_V \phi\frac{\mathrm{d}}{\mathrm{d}t}\left(q\,\mathrm{d}V\right). \end{aligned} \tag{149}$$

The first term of Eq. (148),

$$-\frac{\mathrm{d}}{\mathrm{d}t}\int_{\partial V} \phi\rho_a\mathrm{d}A = -\frac{\mathrm{d}}{\mathrm{d}t}\int_{\partial V_0} \phi\rho_a^0\mathrm{d}A_0, \tag{150}$$

where ρ_a^0 is the referential surface charge such that $\rho_a^0\mathrm{d}A_0 = \rho_a\mathrm{d}A$. Thus,

$$-\frac{\mathrm{d}}{\mathrm{d}t}\int_V \phi q\mathrm{d}V = -\int_{\partial V_0} \dot{\phi}\rho_a^0\mathrm{d}A_0 - \int_{\partial V_0} \phi\frac{\mathrm{d}}{\mathrm{d}t}\left(\rho_a^0\,\mathrm{d}A_0\right) = -\int_{\partial V} \dot{\phi}\rho_a\mathrm{d}A - \int_{\partial V} \phi\frac{\mathrm{d}}{\mathrm{d}t}\left(\rho_a\,\mathrm{d}A\right). \tag{151}$$

Substituting to Eq. (148) we have

$$-\frac{\mathrm{d}}{\mathrm{d}t}\int_{\mathbb{R}^3} \mathbf{D}\cdot\mathbf{E}\mathrm{d}V = -\int_{\partial V} \dot{\phi}\rho_a\mathrm{d}A - \int_{\partial V} \phi\frac{\mathrm{d}}{\mathrm{d}t}\left(\rho_a\,\mathrm{d}A\right) - \int_V \dot{\phi} q\mathrm{d}V - \int_V \phi\frac{\mathrm{d}}{\mathrm{d}t}\left(q\,\mathrm{d}V\right). \tag{152}$$

Substituting into the first law of thermodynamics, Eq. (145), with the use of the expression

for the external work W_0, Eq. (140), we have

$$\begin{aligned}\dot{H} - \frac{\mathrm{d}}{\mathrm{d}t}\int_{\mathbb{R}^3}\frac{\epsilon_0}{2}\mathbf{E}\cdot\mathbf{E}\mathrm{d}V &= \int_V \phi\frac{\mathrm{d}}{\mathrm{d}t}\left(q\,\mathrm{d}V\right) + \int_{\partial V}\phi\frac{\mathrm{d}}{\mathrm{d}t}\left(\rho_a\,\mathrm{d}A\right) + \dot{Q} + \int_V b_i v_i\,\mathrm{d}V + \int_{\partial V} t_i v_i\,\mathrm{d}A \\ &\quad - \int_{\partial V}\dot{\phi}\rho_a \mathrm{d}A - \int_{\partial V}\phi\frac{\mathrm{d}}{\mathrm{d}t}\left(\rho_a\,\mathrm{d}A\right) - \int_V \dot{\phi}q\mathrm{d}V - \int_V \phi\frac{\mathrm{d}}{\mathrm{d}t}\left(q\,\mathrm{d}V\right) \\ &= \dot{Q} - \int_{\partial V}\dot{\phi}\rho_a \mathrm{d}A - \int_V \dot{\phi}q\mathrm{d}V + \int_V b_i v_i\,\mathrm{d}V + \int_{\partial V} t_i v_i\,\mathrm{d}A. \end{aligned} \tag{153}$$

In terms of the external work due to the variations in the electric potential [McMeeking et al., 2007, Cohen et al., 2016]

$$\frac{\mathrm{d}W}{\mathrm{d}t} = \int_V b_i v_i\,\mathrm{d}V + \int_{\partial V} t_i v_i\,\mathrm{d}A - \int_{\partial V}\dot{\phi}\rho_a \mathrm{d}A - \int_V \dot{\phi}q\mathrm{d}V, \tag{154}$$

we end with the expression for the first law of thermodynamics in term of the electric enthalpy

$$\dot{H} - \frac{\mathrm{d}}{\mathrm{d}t}\int_{\mathbb{R}^3}\frac{\epsilon_0}{2}\mathbf{E}\cdot\mathbf{E}\mathrm{d}V = \dot{W} + \dot{Q}. \tag{155}$$

B Chain stress and deriving the chain end-to-end vector by the deformation gradient

In order to evaluate the stress, depicted in section 3.4.1, derivation of the term $\frac{\partial \mathbf{r}}{\partial \boldsymbol{F}}$ is needed. This is carried out in index notation.

The end-to-end vector of the chain in the current configuration is

$$r_i = F_{ip} r_p, \tag{156}$$

where r_i^0 is the end-to-end vector of the chain in the reference configuration and F_{ij} is the deformation gradient. Accordingly

$$\frac{\partial r_i}{\partial F_{kl}} = \frac{\partial}{\partial F_{kl}} \left(F_{ip}\right) r_p^0 = \delta_{ik}\delta_{lp} r_p^0 = \delta_{ik} r_l^0. \tag{157}$$

From Eq. (124), the mechanical stress in the j-th chain is

$$\sigma_{ks}^{\mathrm{m}(j)} = \frac{k\,T}{l}\left(\tau_i^{(j)} \frac{\partial r_i^{(j)}}{\partial F_{kl}}\right) F_{sl} = \frac{k\,T}{l} \tau_i^{(j)} \delta_{ik}\delta_{lp} r_p^{0(j)} F_{sl} = \frac{k\,T}{l} \tau_k^{(j)} F_{sp} r_p^{0(j)} = \frac{k\,T}{l} \tau_k^{(j)} r_s^{(j)}. \tag{158}$$

Since $\tau_k^{(j)} \parallel r_s^{(j)}$(established in section 3.2.3) it follows that

$$\sigma_{ks}^{\mathrm{m}(j)} = \frac{k\,T}{l} \tau^{(j)} r^{0(j)} \hat{r}_k^{(j)} \hat{r}_s^{(j)}. \tag{159}$$

C The initial guess for $\boldsymbol{\tau}$

The Lagrange multiplier $\boldsymbol{\tau}$ is extracted from the implicit equation that follows from the constraint in Eq. (98),

$$\int \hat{\boldsymbol{\xi}}\, p\, \mathrm{d}\Gamma = \frac{\mathbf{r}}{n\, l}, \tag{160}$$

where

$$p\left(\hat{\boldsymbol{\xi}}, h\right) = \frac{1}{Z}\, \exp\left(\boldsymbol{\tau}\cdot\hat{\boldsymbol{\xi}} - \frac{h}{k\, T}\right). \tag{161}$$

Taking the first two terms of Taylor expansion series for $\boldsymbol{\tau}$

$$\boldsymbol{\tau} = \boldsymbol{\tau}_0 + \boldsymbol{A}\mathbf{r} + o\left(r^2\right) \cong \boldsymbol{A}\mathbf{r}, \tag{162}$$

where according to Eq. (75) $\boldsymbol{\tau}_0 = \boldsymbol{\tau}\left(r = 0\right) = 0$.

Thus,

$$\exp\left(\boldsymbol{\tau}\left(\mathbf{r}\right)\cdot\hat{\boldsymbol{\xi}} - \frac{h}{k\, T}\right) \overset{\mathbf{E}\to 0}{\longrightarrow} \exp\left(\hat{\boldsymbol{\xi}}\cdot\boldsymbol{A}\mathbf{r}\right) \cong 1 + A_{ik}\hat{\xi}_i r_k, \tag{163}$$

and

$$Z = \int_{\theta,\phi}\left(1 + A_{ik}\hat{\xi}_i r_k\right)\sin\left(\theta\right)\mathrm{d}\theta\mathrm{d}\phi = 4\pi + A_{ik}\int \hat{\xi}_i \mathrm{d}\Gamma r_k = 4\pi. \tag{164}$$

Hence,

$$p\left(\hat{\boldsymbol{\xi}}, h\right) = \frac{1}{Z}\, \exp\left(\boldsymbol{\tau}\cdot\hat{\boldsymbol{\xi}} - \frac{h}{k\, T}\right) = \frac{1}{4\pi}\, \left(1 + \left(\boldsymbol{A}\mathbf{r}\right)\cdot\hat{\boldsymbol{\xi}}\right), \tag{165}$$

and by taking into account Eq. (165) in Eq. (160)

$$\begin{aligned}\frac{1}{4\pi}\int \hat{\boldsymbol{\xi}}\left(1 + \left(\boldsymbol{A}\mathbf{r}\right)\cdot\hat{\boldsymbol{\xi}}\right)\mathrm{d}\Gamma &= \frac{1}{4\pi}\int \left(\boldsymbol{A}\mathbf{r}\right)\cdot\hat{\boldsymbol{\xi}}\otimes\hat{\boldsymbol{\xi}}\mathrm{d}\Gamma = \frac{1}{4\pi}\left(\frac{4\pi}{3}\boldsymbol{I}\right)\cdot\left(\boldsymbol{A}\mathbf{r}\right)\\ &= \frac{1}{3}\left(\boldsymbol{A}\mathbf{r}\right)\cdot\boldsymbol{I} = \frac{\mathbf{r}}{n\, l} \Longrightarrow \boldsymbol{A} = \frac{3}{n\, l}\boldsymbol{I}.\end{aligned} \tag{166}$$

and $\boldsymbol{\tau}\left(\mathbf{E}\to\mathbf{0}\right)$ is

$$\boldsymbol{\tau} = \boldsymbol{A}\mathbf{r} = \frac{3\mathbf{r}}{n\, l} \tag{167}$$